YAP engages RIF1 to dampen replication stress-induced DNA damage in human squamous cell carcinoma.

Jodie Bojko[1,2], Elodie Sins[3], Benjamin Flynn[1,3], James Scarth[4], Mikal Negasi[5], Bertram Aschenbrenner[6], Molly Guscott[4], Alexander Howard[1,7], Emily Lay[1,8], Emma Bailey[4], Natalia Krajic[6], Marco Franciosi[9,10], Sandra Catalán Jiménez[1,11], Kelli Gallacher[1], Ilaria Di Girolamo[3], Reem Bagabas[3], Caterina Missero[9,10], Jun Wang[4], Sarah McClelland[4], Beate M. Lichtenberger[6], Ute Jungwirth[1,12], Gernot Walko[1,3,*]

[1]Department of Life Sciences, University of Bath, Bath, UK.

[2]Current affiliation: School of Cellular and Molecular Medicine, University of Bristol, Bristol, UK.

[3]Centre for Oral Immunobiology and Regenerative Medicine, Institute of Dentistry, Queen Mary University of London, London, UK.

[4]Barts Cancer Institute, Queen Mary University of London, London, UK.

[5]Translational and Clinical Research Institute, Newcastle University, Newcastle, UK.

[6]Department of Dermatology, Medical University of Vienna, Vienna, Austria.

[7]Current affiliation: Astex Pharmaceuticals, Cambridge, UK.

[8]Current affiliation: Centre for Cell Biology and Cutaneous Research, Blizard Institute, Queen Mary University of London, London, UK.

[9]Department of Biology, University of Naples Federico II, Naples, Italy.

[10]CEINGE – Biotechnologie Avanzate Franco Salvatore S.C.A.R.L., Naples, Italy.

[11]Current affiliation: ONA Therapeutics, Madrid, Spain.

[12]Cancer Research Horizons Therapeutic Innovation, Newcastle Drug Discovery Group, Translational and Clinical Research Institute, Newcastle University, Newcastle, UK.

[*]Correspondence: g.walko@qmul.ac.uk

Summary

Squamous cell carcinoma cells experience high levels of replication stress due to oncogene-induced cell cycle deregulation. How such cells sustain rapid proliferation despite replication stress is still not fully understood. Here, we discovered, using rapid immunoprecipitation mass spectrometry of endogenous protein (RIME) analysis, that the squamous cell carcinoma oncoprotein YAP engages with RIF1, a key regulator of DNA replication and DNA damage repair under replication stress. RIF1 is highly expressed in human squamous cell carcinoma cell lines and tissues and upregulated during tumour progression. Depletion of RIF1 in squamous cell carcinoma cells exacerbates their endogenous replication stress. Mechanistically, we show that YAP interacts with RIF1 specifically at broken replication forks, and that YAP depletion impairs DNA damage repair under replication stress. Our results thus demonstrate that YAP's oncogenic functions in squamous cancers involve both transcriptional and non-transcriptional mechanisms, the latter through interaction with RIF1 to dampen replication stress.

Keywords

Hippo signalling, YAP, TAZ, RIF1, squamous cell carcinoma, replication stress.

Introduction

Squamous cell carcinomas (SCCs) are among the most common solid tumours [1], with cutaneous SCC (cSCC) being the most prevalent type, imposing a major healthcare burden due to its high incidence [2].

Oncogenic signalling drives cancer cell proliferation by interfering with cell cycle control and upregulation of transcription, thereby causing replication stress, which occurs when DNA

50 replication fork progression in S phase slows or stalls [3-5]. Ineffective resolution of
51 replication stress leads to genomic instability or mitotic catastrophes [3, 4]. Cancer cells with
52 high endogenous replication stress rely on DNA damage repair (DDR) for survival [3]. Of
53 note, stem and progenitor cells in healthy human squamous epithelia have already high
54 levels of endogenous replication stress due to their high proliferation rates, and couple
55 activation of DDR pathways to polyploidisation and terminal differentiation as a homeostatic
56 mechanism [6-8]. The same mechanism operates to eliminate pre-cancerous cells [7-9]. In
57 SCC, this protective mechanism is not fully operational, allowing SCC cells to proliferate
58 despite DNA damage [10].

59 RIF1 is a key regulator of DNA replication and DDR [11]. By organising higher order
60 chromatin structures into zones of coordinated DNA replication, and through recruitment of
61 protein phosphatase 1 (PP1) to prevent MCM (minichromosome maintenance complex)
62 subunit phosphorylation, RIF1 suppresses late replicating origin firing [12-19]. Under
63 replication stress, RIF1 has two known functions: it protects stalled replication forks from
64 resection [20-22], and in DDR interacts with BRCA1 at broken replication forks [23]. While
65 RIFs role in non-homologous end joining (NHEJ) is well documented [24-27], its role in DNA
66 replication under replication stress is underexplored.

67 The transcriptional co-regulators Yes-associated protein (YAP) and transcriptional co-
68 activator with PDZ-binding motif (TAZ, also called WW Domain Containing Transcription
69 Regulator 1 (*WWTR1*)) are essential oncoproteins in SCC [28-30]. YAP/TAZ operate as
70 transcriptional co-activators and co-repressors by indirectly binding to DNA via different
71 transcription factors (TFs; predominantly those of the TEAD family [28]) [31]. While YAP is
72 essential in squamous epithelial stem cell proliferation upon injury [32, 33], overexpression

73 of oncogenic YAP induces rapid senescence [33]. It is likely that this oncogene-induced
74 senescence mechanism is linked to increased YAP-driven transcription, causing transcription-
75 replication conflicts and replication stress [34, 35].

76 How YAP/TAZ control oncogenic signalling in human SCC at the molecular level, and how
77 human SCC cells deal with oncogene-induced replication stress remains poorly understood.
78 Using a multi-omics approach we characterized transcriptional and non-transcriptional
79 mechanisms of YAP's oncogenic role in human SCC. We identified RIF1 as a binding partner
80 of YAP in human SCC cells, expanding its known interaction in early amphibian development
81 to human cancers. Importantly, our finding that YAP engages RIF1 under replication stress
82 and facilitates DDR has translational implications, since replication stress is a crucial
83 vulnerability of cancer cells that can be exploited therapeutically.

84

85 **Materials and Methods**

86 Complete details of the materials and methods are provided in the supplemental materials
87 and methods.

88

89 **Results**

90 ***YAP/TAZ-TEAD-mediated oncogenic signalling balances proliferation and differentiation***
91 ***and drives metastatic progression of human squamous cell carcinoma.***

92 In healthy epidermis, YAP/TAZ balance cell proliferation and terminal differentiation [32, 36].
93 To test if YAP/TAZ play similar roles in cSCC, we performed RNAseq analysis on SCC13 cells, a
94 widely used human cSCC cell line [37], following acute siRNA-mediated knockdown of
95 YAP/TAZ (siYAP/TAZ; Supplementary Fig. 1A, B). While we were unable to significantly

96 deplete TAZ (*WWTR1*), the TAZ-targeting siRNA pool prevented compensatory upregulation
97 of TAZ in response to YAP knockdown (Supplementary Fig. 1B) [32]. DESeq2 analysis revealed
98 a large number of differentially expressed genes (DEGs) upon siYAP/TAZ (977 DEGs
99 downregulated, 2,209 DEGs upregulated; Supplementary Table 1). Downregulated DEGs
100 comprised both, genes positively regulated by YAP/TAZ in cooperation with TEADs [38], and
101 genes regulated by YAP/TAZ in cooperation with the Myb-MuB (MMB) complex [39]
102 (Supplementary Fig. 1C and Supplementary Table 1). Gene set enrichment analysis (GSEA)
103 revealed significant enrichment of pathways associated with cell cycle regulation, DNA
104 replication, and mitosis among the downregulated DEGs, and of pathways associated with
105 keratinization, cornification, extracellular matrix (ECM) remodelling, and immunoregulation
106 among the upregulated DEGs (Supplementary Figs. 1D, E, and Supplementary Table 1).
107 YAP/TAZ knockdown also led to increased terminal differentiation which was evident from (i)
108 enrichment of an epidermal terminal differentiation gene signature [40] in the upregulated
109 DEGs and of an epidermal progenitor cell signature [40] in the downregulated DEGs
110 (Supplementary Fig. 2A), and (ii) upregulation of transcriptional regulators of terminal
111 differentiation and genes belonging to the epidermal differentiation complex (EDC) [41]
112 (Supplementary Fig. 2B and Supplementary Table 1).

113 We next used the YAP/TAZ target gene expression signature derived from our RNA-seq data
114 to perform gene set variation analysis (GSVA) on one of the largest bulk RNA-seq datasets
115 from patients with cSCC (237 patients) [42]. This revealed that genes that are positively
116 regulated by YAP/TAZ in SCC13 cells are expressed significantly higher in cSCC tumours (as
117 well as their perilesional skin tissue) that have progressed to metastatic disease, compared
118 to those cSCC tumours that have not (Fig. 1A). Genes that were positively regulated by

119 YAP/TAZ in SCC13 cells were also highly expressed in cSCC metastases. Conversely, genes
120 that were negatively regulated by YAP/TAZ in SCC13 cells, including those genes related to
121 terminal differentiation, displayed significantly reduced expression in cSCCs that had
122 progressed to metastatic disease, as well as in the respective metastases (Fig. 1B). This
123 finding provides intriguing evidence in clinical samples for the involvement of YAP/TAZ in the
124 metastatic progression of human cSCC.

125 In accordance with the detected transcriptomic changes in siYAP/TAZ SCC13 cells, we
126 observed that cell proliferation was strongly reduced upon expression of doxycycline-
127 inducible YAP-targeting shRNAs (shYAP) (Fig. 1C). This was evident from reduced levels of
128 Ser10-phosphorylated histone H3 (pHH3), a marker of mitotic cells, and strong upregulation
129 of the CDK inhibitor p21 (Fig. 1D). Consistent with p21 upregulation (Fig. 1D, Supplementary
130 Fig. 2C) and the reduced expression of several key regulators of DNA replication
131 (Supplementary Fig. 1C and Supplementary Table 1), most shYAP SCC13 cells arrested in G1,
132 and a much smaller proportion of cells progressed through S phase (Fig. 1E). Compromised
133 cell cycle progression and increased terminal differentiation led to reduced 2D clonal growth
134 (Fig. 1F) and 3D spheroid growth (Fig. 1G) of shYAP SCC13 cells. The effects of shTAZ on
135 SCC13 proliferation were less strong (Figs. 1D, F). To assess if in cSCC cells YAP/TAZ were
136 driving oncogenic transcription through TEAD TFs, we employed the potent allosteric pan-
137 TEAD inhibitor GNE-7883 [43]. GNE-7883 reduced proliferation of SCC13 cells and other
138 cSCC cell lines in dose-dependent manner (Figs. 2A, B). GNE-7883 treatment of SCC13 cells
139 phenocopied shYAP by strongly inducing p21 and the terminal differentiation marker
140 involucrin, and downregulating pHH3 (Figs. 2C, D). GNE-7883 also effectively blocked
141 proliferation of SCC13 cells growing as 3D spheroids (Figs. 2E, F). Consistent with

142 *CDKN1A*/p21 being a major effector of disrupted YAP/TAZ-TEAD signalling, we found that
143 SCC13 cells expressing *CDKN1A*-targeting shRNAs were able to proliferate normally upon
144 GNE-7883 treatment (Figs. 2G, H). We conclude that YAP/TAZ-TEAD regulate the balance
145 between proliferation and terminal differentiation, thereby promoting a highly proliferative
146 and undifferentiated cell state that is relevant for disease progression. This important
147 function is conserved between normal epidermal keratinocytes [32, 36] and neoplastic
148 keratinocytes of both BCC [44] and cSCC (this study).
149
150 ***YAP/TAZ-TEAD-mediated oncogenic signalling is major contributor to replication stress in***
151 ***squamous cell carcinoma cells.***
152 Reduced activation of the replication stress checkpoint (phosphorylation of CHK1 on Ser317;
153 [45, 46]) was evident in SCC13 cells upon shYAP but not shTAZ knockdown (Supplementary
154 Fig. 3A), while depletion of either YAP or TAZ decreased the levels of γH2AX. In the context
155 of replication stress, γH2AX marks accumulation of DNA double strand breaks (DSBs) at
156 collapsed replication forks [6, 23, 46] (Supplementary Fig. 3A). Furthermore, using mRNA
157 expression data from the DepMap project [47], we discovered a strong correlation between
158 the expression of a replication stress signature [48] and an SCC-specific YAP/TAZ activity
159 signature comprising 10 highly-correlated YAP/TAZ target genes from our RNAseq dataset in
160 HNSCC (Supplementary Table 1, Supplementary Figs. 4A–D). To provide additional evidence
161 for a causal link between oncogenic YAP signalling and replication stress, we overexpressed
162 wildtype YAP and hyperactive YAP5SA and YAPS127A mutants [33] in SCC cells. As shown in
163 Supplementary Fig. 3B, all three YAP transgenes increased YAP's transcriptional output, as
164 evident from strongly elevated expression of the canonical YAP/TAZ-TEAD target gene *CCN1*,
165 and notably reduced cell proliferation when compared to empty vector control

166 (Supplementary Fig. 3C). Both wildtype YAP and YAPS127A enhanced replication stress, as
167 evident from increased γH2AX expression and increased CHK1 Ser345 phosphorylation [45,
168 46], while YAP5SA overexpression caused increased p21 expression, probably indicating
169 oncogene-induced senescence (Supplementary Fig. 3B).

170 To demonstrate that transcription can be a general contributor to replication stress in SCC
171 cells, we transiently inhibited RNA synthesis in SCC13 cells using triptolide before assessing
172 γH2AX levels [49]. Triptolide treatment reduced RNA synthesis (Supplementary Fig. 3D) and
173 γH2AX expression to a similar extend as TEAD inhibition by GNE-7883 (Supplementary Figs.
174 3E, F). Together, these findings showed that YAP/TAZ-TEAD-driven oncogenic signalling is a
175 major contributor to the endogenous replication stress of SCC cells.

176

177 ***A fraction of chromatin-associated YAP interacts with RIF1.***

178 To understand how YAP executes its transcriptional roles, we performed rapid
179 immunoprecipitation mass spectrometry of endogenous protein (RIME) analysis [50] in
180 SCC13 cells and normal human epidermal keratinocytes (NHK) (Fig. 3), using a knockdown-
181 validated YAP-specific antibody that does not recognise TAZ (Supplementary Figs. 5A, B, G).
182 YAP immunoprecipitation (IP) efficiency was consistently high across all YAP-RIME replicates,
183 with high YAP peptide coverage (63-65%) detected by mass spectrometry analysis
184 (Supplementary Fig. 5C and Supplementary Table 2). Upon stringent filtering of the mass
185 spectrometry data (see Supplementary Materials and Methods) YAP-RIME enabled
186 identification of 47 and 14 high confidence YAP-interacting proteins in SCC13 cells (Fig. 3A,
187 Supplementary Table 2) and NHK cells (Supplementary Fig. 5D and Supplementary Table 2),
188 respectively. Significantly enriched gene ontology terms were all related to processes
189 occurring in the nucleus in both interactomes (Fig. 3B, Supplementary Fig. 5E). Among the

190 SCC13 YAP-interacting proteins were several known regulators of YAP, including
191 Neurofibromatosis type (NF2) [51], Angiomotin-like 1 (AMOTL1) [52], PPP1CB [53], and
192 Prolyl 4-Hydroxylase subunit alpha 2 (P4HA2) [54] (Fig. 3A). Our YAP-RIME also identified
193 several subunits of the BAF-type SWI/SNF chromatin remodelling complex (ARID1A,
194 SMARCA4, SMARCC1, SMARCE1, SMARCD2) [55], and key components of the NuRD
195 chromatin remodelling complex, Chromodomain-helicase-DNA-binding protein 4 (CHD4)
196 and Metastasis Associated 1 Family Member 2 (MTA2). While key components of the
197 general transcriptional machinery (POLR2A, POLR2B, GTF21, TOP1) were present in the
198 SCC13 YAP interactome, TEAD TFs were notably absent (Fig. 3A). A closer inspection of our
199 mass spectrometry data revealed that TEADs, as well as other known YAP-interacting
200 transcription factors, such as JunB and TP63 [56, 57], had been identified but did not pass
201 our stringent bioinformatics filtering criteria (Supplementary Table 2). The overall poor
202 identification of TFs by our YAP-RIME was likely due to their insufficient crosslinking to the
203 DNA by formaldehyde alone, as previously observed for the highly dynamic transcription
204 factor NFκB [58].

205 To identify physiologically relevant interactions, the YAP-interacting proteins were compared
206 to candidate positive and negative regulators of cell proliferation and survival identified in a
207 prior genome-wide RNA screens in SCC13 [32]. This revealed that 22 out of the 47 high
208 confidence YAP-interacting proteins were likely relevant for cell proliferation and/or survival
209 (Fig. 3A, Supplementary Table 2).

210 Our attention was drawn to RIF1, given its recent identification as a non-transcriptional YAP
211 interaction partner in a developmental context in *Xenopus laevis* [59]. We detected RIF1 as a
212 YAP-chromatin-interacting protein in both the SCC13 and NHK YAP-RIME experiments (Fig.

213 3A, Supplementary Fig. 5D) with a much stronger enrichment in SCC13 YAP (Supplementary
214 Fig. 5F and Supplementary Table 2). Of note, PPP1CB, one of the three catalytic subunits of
215 PP1—a key effector of RIF1 [13, 16, 17, 19], was also present in the SCC13 YAP-RIME (Fig. 3A,
216 Supplementary Table 2). Like YAP, RIF1 featured among the positive regulators of cell
217 proliferation and survival of SCC13 cells identified in the aforementioned genome-wide RNA
218 interference screen [32] (Fig. 3A, Supplementary Table 2). As expected, YAP and RIF1 were
219 both localised in the nucleus of SCC13 cells (Fig. 3C) and present in chromatin fractions
220 (Supplementary Fig. 5G), confirming their chromatin-association. To biochemically validate
221 the YAP-RIF1 interaction, co-IP experiments were performed under native non-cross-linking
222 conditions using a different YAP-specific antibody (Supplementary Fig. 6A). Indeed, RIF1
223 could be immunoprecipitated together with YAP from both, whole-cell detergent extracts
224 and nuclei-enriched fractions (Figs. 3D, E). Further validating our RIME results, CHD4 and
225 ARID1A also co-immunoprecipitated with YAP under native conditions. Under these
226 conditions, TEAD transcription factors could also be immunoprecipitated together with YAP
227 (Fig. 3E). In-situ proximity ligation assays (PLA) confirmed very close YAP-RIF1 proximity in
228 the nucleus of SCC13 cells (Fig. 3F). To achieve a sufficiently strong knockdown of both YAP
229 and TAZ to control for PLA signal specificity, we combined our doxycycline-inducible YAP-
230 targeting shRNAs with an siRNA pool targeting YAP and TAZ (Fig. 3F, Supplementary Fig. 6B).
231 The YAP-RIF1 PLA signal was significantly decreased upon YAP/TAZ knockdown. Consistent
232 with our co-IP results, YAP was also found in very close proximity to TEAD1 in the nucleus of
233 SCC13 cells by PLA (Fig. 3G). The YAP-RIF1 PLA signal was completely absent when the two
234 primary antibodies were omitted (Supplementary Figs. 6C, D) and also largely absent from
235 mitotic chromosomes (Supplementary Fig. 6E). To test if the YAP-RIF1 interaction also
236 occurred in other types of SCC, we used the lung SCC (LUSC) cell line HARA. Co-IP was

237 performed with nuclei-enriched HARA cell fractions treated with Benzonase nuclease to
238 enzymatically digest DNA and RNA (Supplementary Figs. 6F, G), demonstrating that YAP and
239 RIF1 are not co-immunoprecipitated because of a DNA bridge between the two proteins. In
240 summary, our results show that RIF1 is a binding partner of chromatin-associated YAP in
241 both healthy human NHKs and cancerous cSCC and LUSC cells.
242
243 ***YAP/TAZ-TEAD modulate RIF1 protein levels.***
244 Our RNAseq analysis revealed that *RIF1* mRNA expression was moderately downregulated in
245 response to siYAP/TAZ (Supplementary Fig. 1A and Supplementary Table 1). A similar, albeit
246 statistically not significant trend could be confirmed in independent siYAP/TAZ samples by
247 RT-qPCR analysis (Fig. 4A). These mild effects of YAP depletion on *RIF1* mRNA expression are
248 likely indirect and may be linked to cell cycle de-regulation. Depletion of RIF1 did not impact
249 on expression of most of the DEGs seen upon siYAP/TAZ (Supplementary Figs. 1B, C, and 2B,
250 C), ruling out a direct involvement in YAP/TAZ-TEAD-controlled transcription.

251 The stability of a protein within a complex often depends on other components of the
252 complex, as proper folding of one protein may require interactions with its partners. RIF1
253 protein expression was lower in siYAP/TAZ compared to siNTC SCC13 cells (Fig. 4B).
254 Conversely, overexpression of wildtype and oncogenic YAP variants increased RIF1 protein
255 levels irrespective of their effects on the cell cycle (pHH3) (Fig. 4C). Interestingly, short-term
256 treatment (24 h) with GNE-7883 to disrupt YAP/TAZ-TEAD binding reduced RIF1 protein
257 expression without affecting *RIF1* mRNA levels (Figs. 4D, E). This suggests that YAP might
258 modulate RIF1 protein levels in a complex with TEADs. Indeed, combined siRNA-mediated
259 knockdown of TEAD1, 3, and 4 (siTEAD1/3/4) in SCC13 cells reduced RIF1 protein to levels
260 similar to those observed in siYAP/TAZ cells (Figs. 4F, G). Interestingly, depletion of YAP

261 impacted chromatin-associated RIF1 levels specifically during S phase (Figs. 4H, I). Since the
262 data presented in Figs. 3E–G showed that YAP is in complex with RIF1 and TEADs, these
263 findings thus suggest that YAP-TEAD modulate protein levels of a fraction of chromatin-
264 associated RIF1 in S phase.

265

266 ***RIF1 is highly expressed in squamous cell carcinoma and upregulated during tumour***
267 ***progression.***

268 To understand if RIF1 contributes to squamous carcinogenesis, we assessed RIF1 protein
269 expression in a panel of human cSCC cell lines, which also included an isogenic cSCC
270 progression series (PM1, MET1–4), including the pre-malignant PM1 precursor lesion [60].
271 Increased RIF1 protein levels were notable in all cSCC cell lines when compared to NHKs (Fig.
272 5A). Consistent with our findings that YAP-TEAD modulate RIF1 protein levels (Fig. 4), RIF1
273 protein expression was highest in SCC13 cells featuring high nuclear YAP levels [32], as also
274 indicated by a low ratio of S127-YAP to total YAP (Fig. 5A). All cSCC lines displayed higher
275 levels of γH2AX compared to NHKs, indicating increased endogenous replication stress (Fig.
276 5A).

277 To investigate if high RIF1 expression was a general hallmark of cancers originating from
278 epidermal keratinocytes, we quantified the levels of RIF1 protein in a tissue array
279 comprising cSCCs of different differentiation grades, as well as different types of BCCs (Figs.
280 5B, C). We detected increased numbers of RIF1-expressing cells within the keratin-positive
281 tumour cell masses of both BCC and cSCC compared to normal skin epidermis, especially
282 within the more aggressive tumour types of infiltrative BCC and poorly differentiated cSCC
283 (Figs. 5B, C). These data are corroborated by immunohistochemistry data from the Human

284 Protein Atlas, depicting increased numbers of RIF1-expressing tumour cells in cSCC, HNSCC
285 and cervical SCC (Supplementary Figs. 7A–C). To obtain a pan-cancer overview of RIF1
286 expression, we used the UALCAN portal [61] to access protein expression data from the
287 Clinical Proteomic Tumour Analysis Consortium (CPTAC) [62]. In HNSCC, RIF1 protein
288 expression increased with tumour grade (Fig. 5D) and RIF1 expression was higher across
289 several cancer types compared to normal tissue (Supplementary Fig. 7D). The UALCAN
290 portal also allows assessment of the impact of somatic alterations (small mutations or copy
291 number alterations) in signalling pathways on the cancer proteome [61, 62]. We found that
292 in both HNSCC (Fig. 5E) and LUSC (Supplementary Fig. 7E) increased RIF1 protein expression
293 predominantly correlated with somatic Hippo pathway alterations, in contrast to alterations
294 in other signalling pathways, implying altered Hippo pathway activity in the regulation of
295 RIF1 expression. In contrast, in other cancer types, alterations in pathways other than Hippo
296 signalling had a strong impact on increased tumour expression of RIF1 (Supplementary Figs.
297 7F, G). Collectively, our multi-omics analysis confirm a close relationship between Hippo
298 signalling and RIF1 protein expression and point towards a role of RIF1 in squamous cell
299 carcinogenesis.
300
301 ***Depletion of RIF1 increases replication fork speed in squamous cell carcinoma cells.***
302 Consistent with a role of RIF1 in controlling S phase progression of SCC cells, we observed
303 that on release from a double thymidine block, shRIF1 SCC13 cells progressed more rapidly
304 through S phase (Fig. 6A). Phosphorylation levels of MCM2 and MCM4 proteins, targets of
305 the Dbf4-dependent kinase (DDK; composed of CDC7 kinase and its activator, DBF4) [16,
306 18], were increased in RIF1-depleted SCC13 cells in a RIF1 dosage-dependent manner (Figs.
307 6B, C), particularly in early and mid S phase (2- and 4-h time points post-dTb, Fig. 6C),

308 indicating alterations in the dynamics of origin firing [16-19]. Accordingly, chromatin loading
309 of PCNA, which is required for DNA replication after the action of CDC7, was also increased
310 during early and mid S phase of shRIF1 SCC13 cells (Fig. 6C). Therefore, the faster
311 progression of SCC13 cells through S phase after RIF1 depletion likely reflects an increase in
312 DNA replication initiation events in early and mid S phase [16, 18]. We also examined DNA
313 replication dynamics in shRIF1 cells using a novel long-read sequencing method, DNAscent
314 [63]. We discovered that RIF knockdown increased fork speed along with led to longer
315 replication tracks (Figs. 6D, E, and Supplementary Figs. 8A, B).
316
317 ***RIF1 protects against endogenous replication stress in squamous cell carcinoma cells.***
318 Under replication stress, RIF1 protects stalled replication forks [16, 20-22], but also
319 facilitates homology-mediated DDR at broken replication forks [23]. The elevated expression
320 of RIF1 in SCC cells could therefore indicate a role for RIF1 in enabling the cells to deal with
321 high levels of endogenous replication stress that are, at least in part, controlled by YAP-
322 TEAD-driven oncogenic mechanisms (Fig. 2). Indeed, we found a strong correlation between
323 *RIF1* expression and a replication stress signature [48] in HNSCC cell lines (Supplementary
324 Figs. 4A, E). In contrast to a slowing down or stalling of replication fork progression, which is
325 frequently observed when cells experience replication stress [3-5], our DNAscent analysis
326 revealed increased replication fork speed upon RIF knockdown (Figs. 6D, E). Moreover,
327 replication fork stalling or pausing, as defined by a shift of DNAscent 'stall score' distribution
328 closer to 1.0, was not detected (Fig. 6F). Previous studies have found that increased
329 replication speed can lead to DNA damage, whereby faster replication forks have
330 insufficient time to recognize damaged DNA in need of repair [64, 65]. The only moderate
331 activation of CHK1 (phosphorylation on Ser317 and S345; [45, 46]) and very mild increase of

332 ATR-mediated S33-phosphorylation of RPA32 [46] in shRIF1 SCC13 cells, in contrast to the
333 strongly elevated levels of γH2AX and hyperphosphorylated pS4/8-RPA32 (indicating
334 phosphorylation by ATM and DNA-PK in response to generation of DNA DSBs [46, 66, 67]
335 (Figs. 7A, B) are corroborating such a scenario. Indeed, replication fork collapse and
336 concomitant activation of ATM/DNA-PK signalling were previously observed in response to
337 ATR inhibition in cells experiencing hydroxyurea (HU)-induced replication stress [67]. It is
338 worth noting that DNAScent only detects short (<20 min) replication fork stalls/pauses and
339 currently cannot measure longer fork stalls and fork breakage. Given that RIF1 facilitates
340 repair of broken replication forks [23] it is likely that loss of this additional function also
341 contributes to the increased accumulation of DNA damage in shRIF1 cells. Because the
342 replication checkpoint was not robustly activated in shRIF1 SCC13 cells (Figs. 7A, B), they
343 were able to progress through the cell cycle despite persistent DNA damage (Figs. 7C, D). A
344 small increase in the G2/M fraction in shRIF1 SCC13 cells (Figs. 7C, D) was noticeable as well
345 as a slightly elevated pHH3 expression in siRIF1 cells (Fig. 7E). The accumulation of DNA
346 damage in cultures of shRIF1 SCC13 cells became more accentuated after a few passages,
347 when cells had undergone multiple rounds of cell division (Fig. 7F), ultimately resulting in
348 reduced clonal growth (Figs. 7G, H). To confirm that the replication stress-protecting effect
349 of RIF1 is conserved in other types of SCC, we depleted RIF1 in the HNSCC cell line SAS,
350 which displays a strong correlation between RIF1 expression and replication stress
351 (Supplementary Fig. 4E) and carries a *YAP-MAML2* gene fusion resulting in a hyperactive
352 YAP variant [68]. Indeed, we observed a dosage-dependent effect of shRIF1 on cell viability
353 (Supplementary Figs. 9A–C) and DNA damage (Supplementary Figs. 9D, E). Decreased cell
354 viability (Supplementary Fig. 9F) and increased γH2AX levels (Supplementary Fig. 9G) were
355 also detected in the LUSC cell line HARA upon shRIF1. Together, our results point to a

356 scenario where SCC cells depend on elevated RIF1 expression to dampen their high levels of
357 endogenous replication stress.
358
359 ***YAP is involved in DNA damage repair at collapsed replication forks.***
360 Our discovery of RIF1 as a YAP interaction partner in human SCC cells raised the exciting
361 possibility that in this cancer context, YAP could play dual roles in both transcription and
362 DNA replication under replication stress. To test, if YAP, like RIF1, might function at
363 collapsed replication forks [23], we treated SCC13 cells with 4 mM HU [23, 69] for 24 h. This
364 triggered strong activation of the replication stress checkpoint (phosphorylation of CHK1 on
365 Ser317; [45, 46]) and accumulation of DNA DSBs, marked by strongly elevated γH2AX
366 expression (Fig. 8A). Persisting γH2AX expression following HU washout indicated
367 accumulation of DNA damage at stalled and subsequently inactivated replication forks [69]
368 (Fig. 8A). This was further confirmed by the presence of RAD51 foci [23] (Fig. 8B) and
369 appearance of pan-nuclear γH2AX staining, indicating severe DNA replication stress [70],
370 upon 24 h HU treatment (Supplementary Fig. 10A). Indeed, some cell death (appearance of
371 sub-G1 fraction in EdU/PI cell cycle profiles, Supplementary Fig. 10A) was noticeable from 15
372 h HU treatment onwards. Interestingly, YAP protein levels were increased following washout
373 of HU after 24 h of treatment, suggesting a potential role of YAP in DDR upon replication
374 fork collapse (Fig. 8C). Indeed, while the YAP-RIF1 PLA signal remained unchanged upon
375 short-term (3 h) HU treatment, it increased significantly after long-term (24 h) HU treatment
376 (Fig. 8D). Moreover, upon long-term HU treatment, more YAP molecules were found in
377 close vicinity of γH2AX by in-situ PLA (Fig. 8E, Supplementary Fig. 10C), suggesting that YAP
378 associates with RIF1 preferentially near DNA DSBs at broken replication forks. To test if YAP
379 is directly involved in DDR at broken replication forks, we optimized conditions for RNA

380 interference experiments to only minimally perturb the cell cycle in response to siYAP/TAZ
381 (Fig. 8F, Supplementary Fig. 10D). For these experiments, HU concentration was reduced to
382 2 mM to avoid potential confounding effects of HU-induced cell death. As shown in Fig. 8F,
383 by 48 h post-transfection with a low concentration of siYAP/TAZ (1 nM), SCC13 cells
384 displayed reduced levels of YAP and only modest upregulation of p21 and downregulation of
385 pHH3, while γH2AX levels (as a read-out of YAP-TEAD-driven replication stress) were
386 strongly reduced. Treatment with 2 mM HU during the last 24 h post-siYAP/TAZ transfection
387 led to prominent S phase arrest, as evident from strongly reduced pHH3 levels and
388 replication stress checkpoint activation (phosphorylation of CHK1 on Ser345) (Fig. 8F).
389 Under these conditions, YAP depletion did not cause a decrease in γH2AX levels but instead
390 led to a significant increase in comparison to untreated siYAP/TAZ cells (Fig. 8F). Since
391 transcription is globally dampened under high concentrations of HU [71] and YAP was
392 depleted specifically during the HU treatment period, these findings suggest a novel non-
393 transcriptional function of YAP where it is involved in DDR at broken replication forks.

394 Given the dual function of YAP in promoting TEAD-mediated transcription and facilitating
395 DDR under severe replication stress, we examined if pharmacologically induced replication
396 stress could act synergistically with YAP depletion to impair SCC proliferation. Of note, HU is
397 sometimes used in chemoradiotherapy for HNSCC patients [72]. Indeed, we observed a
398 synergistic effect of shYAP and low doses of HU on SCC13 clonal colony growth (Figs. 8G, H).
399 This finding highlights the possibility of using pharmacological replication stress inducers in
400 combination with YAP-TEAD inhibitors [73] to treat SCC.

401

402 **Discussion**

403 Our findings provide novel insight into the oncogenic mechanisms of hyperactive YAP/TAZ in
404 SCC. While YAP/TAZ promote proliferation by regulating transcriptional programmes that
405 drive cell cycle progression, they also suppress commitment to terminal differentiation.
406 Thus, the functions of YAP/TAZ are highly conserved within the epidermal lineage, as both
407 normal epidermal stem cells [32, 33, 36] and neoplastic keratinocytes in BCC [44] and cSCC
408 (this study) show strong dependency on YAP/TAZ-TEAD signalling for cell proliferation. This
409 suggests that cancers originating from epidermal stem/progenitor cells 'hijack' the tissue
410 regenerating functions of YAP/TAZ to fuel their high rates of proliferation while remaining in
411 an undifferentiated cell state. The increased expression of genes that are positively
412 regulated by YAP/TAZ in tumour tissue of human cSCCs that underwent metastatic
413 progression (Fig. 1) provides strong support for this idea. Our RIME analysis revealed that
414 the transcriptional co-regulator functions of YAP/TAZ are likely mediated by the BAF-type
415 SWI/SNF and the NuRD chromatin remodelling complexes. Indeed, in HNSCC cells, BAF-type
416 SWI/SNF and YAP-TEAD complexes were shown to be co-dependent for chromatin binding,
417 whereby they create a positive-feedback mechanism to maintain open chromatin for
418 transcription [74]. In contrast, recruitment of the NuRD complex [75] could be involved in
419 the observed co-repressor functions of YAP/TAZ.

420 In a previous study which employed a transgenic mouse model of cSCC development,
421 simultaneous activation of oncogenic $Kras^{G12D}$ and knock-down of YAP/TAZ in epidermal
422 stem cells was found to induce apoptosis [76]. In contrast, we found that YAP/TAZ depletion
423 in human SCC has cytostatic- and differentiation-promoting, rather than cytotoxic effects,
424 which appear to be mediated by induction of p21. It is worth noting that activating
425 mutations in the *RAS* proto-oncogenes are not very frequent in human cSCC [2], with some

426 tumours (~10%) showing copy number loss of *HRAS* [77]. Induction of apoptosis in response
427 to YAP/TAZ depletion might thus be specific to SCCs expressing oncogenic RAS [76].

428 We show that a key function of RIF1 in human squamous cancers is to regulate DNA
429 replication dynamics. Our findings in SCC13 cells show that in the absence of RIF1, origin
430 firing and replication fork speed are increased (Fig. 6). However, our DNAscent analysis
431 revealed that the rate of replication fork stalling/pausing in SCC13 cells was not increased by
432 RIF1 depletion. A previous study found that replication stress can be caused by increased
433 fork speed and without fork stalling when the average fork velocity increases above a ~40%
434 gain [64]. Although the average increase in fork speed in shRIF1 SCC13 cells was only ~25%,
435 we believe that this increased fork speed can generate increasing levels of replication stress
436 and DNA damage over a few cell division cycles, as was previously shown for cells with
437 elevated E2F-driven transcription [78].

438 Since origin firing occurs preferentially within open chromatin regions that contain
439 transcriptional-regulatory elements, some of which were shown to be enriched for TEAD TF
440 binding motifs [79], modulation of RIF1 chromatin association by YAP-TEAD (Fig. 4) could
441 serve to coordinate YAP-TEAD-driven transcription with DNA replication. Unfortunately,
442 because of the confounding effects of YAP depletion on the cell cycle (Fig. 1), it was not
443 possible for us to assess if YAP was involved in DNA replication under unperturbed
444 conditions.

445 An important discovery of our study was a specific role of YAP in facilitating DDR at
446 deactivated replication forks under severe replication stress. How YAP might work together
447 with RIF1 to promote DDR at broken replication forks remains elusive at this point,
448 particularly since the mechanism by which RIF1 enables BRCA1/RAD51-dependent repair of

449 broken replication forks it yet not well understood [23]. Notably, this DDR function is
450 attributed specifically to the long isoform of RIF1 (RIF1-long), while control of replication
451 dynamics is mediated by both RIF1-long and RIF1-short isoforms [80].

452 Our findings thus provide evidence for a non-canonical, non-transcriptional role of YAP in
453 SCC, whereby it engages RIF1 to dampen the high levels of endogenous replication stress in
454 these cancers, which are—at least in part—caused by YAP's oncogenic functions itself.
455 Induction of replication stress together with pharmacological YAP/TAZ-TEAD inhibition [73]
456 could thus potentially be used as a combination therapy strategy to treat SCC.

457

458 **Funding information**

459 This work was supported by the UK Research & Innovation (UKRI) Biotechnology and
460 Biological Sciences Research Council (BBSRC, grant BB/T012978/1 to Gernot Walko), the UK
461 Research & Innovation (UKRI) Medical Research Council (MRC, grant MR/W031442/1 to
462 Sarah McClelland), the Academy of Medical Sciences (grant SBF005\1005 to Gernot Walko),
463 the British Skin Foundation (grants 004/SG/18, 036/S/18 ('Peter Massey Skin Cancer Grant')
464 and 011_SG_22 to Gernot Walko), the Royal Society (grant RGS\R1\191087 to Gernot
465 Walko), the LEO Foundation (grant LF-AW_EMEA-21-400116 to Beate Lichtenberger), the
466 City of Vienna Fund for Innovative Interdisciplinary Cancer Research (grant 22059 to Beate
467 Lichtenberger), the Austrian Science Fund (FWF) (grant 36368-B to Beate Lichtenberger),
468 Cancer Research UK (CRUK, grant DRCPFA-Jun24/100005 to Sarah McClelland), and the
469 Italian Association for Cancer Research (AIRC, grant IG25116 to Caterina Missero). Ute
470 Jungwirth gratefully acknowledges funding from Cancer Research UK (Newcastle Drug
471 Discovery Unit Programme Grant DRCDDRPGMApr2020\100002). Gernot Walko, Jun Wang,
472 Elodie Sins, Benjamin Flynn, and Emma Bailey also acknowledge funding support from the

Barts Charity (UK) Strategic Award to the Barts Centre for Squamous Cancer (Centre grant 'A Centre of Excellence for Squamous Cancer', grant G-002030). Jun Wang and Emma Bailey further acknowledge funding support from the Cancer Research UK City of London Major Centre Award core funding support to the Barts Cancer Institute. Jodie Bojko was recipient of a Raoul & Catherine Hughes Scholarship through the University of Bath 'Alumni and Friends' network. Reem Bagabas was recipient of a PhD studentship from the Saudi Arabian Cultural Bureau.

Acknowledgements

We would like to thank all members of the Walko and Jungwirth labs for their inputs. We wish to thank our colleagues from the Barts Centre for Squamous Cancer at Queen Mary University of London for critical feedback on our draft manuscript. We thank Genomics Birmingham Genomics Service at the University of Birmingham, for the generation of the DNAscent data. We also acknowledge support from the bioimaging facility of the Barts Cancer Institute (Queen Mary University of London).

Author contributions

Jodie Bojko: Data Curation, Formal Analysis, Investigation, Methodology, Visualization, Writing: Original Draft Preparation; Writing: Review & Editing; Elodie Sins: Data Curation, Investigation, Methodology; Benjamin Flynn: Data Curation, Formal Analysis, Investigation, Methodology, Software, Validation, Visualization; James Scarth: Data Curation, Formal Analysis, Investigation, Methodology, Visualization; Mikal Nigasi: Data Curation, Formal Analysis, Investigation, Methodology, Visualization; Bertram Aschenbrenner: Data Curation, Formal Analysis, Investigation, Methodology, Software, Visualization; Molly Guscott: Formal

Analysis, Investigation, Methodology, Software; Alexander Howard: Formal Analysis, Investigation, Methodology; Emily Lay: Formal Analysis, Investigation, Methodology; Emma Bailey: Formal Analysis, Investigation, Methodology, Software, Visualization; Natalia Krajic: Investigation, Methodology; Marco Franciosi: Investigation, Methodology; Sandra Catalan: Investigation, Methodology; Kelli Gallacher: Investigation, Methodology; Ilaria di Girolamo: Data Curation, Investigation; Reem Bagabas: Data Curation, Investigation; Caterina Missero: Funding acquisition, Resources, Supervision, Validation; Jun Wang: Funding acquisition, Methodology, Resources, Supervision; Sarah McClelland: Funding acquisition, Resources, Supervision, Validation; Beate Lichtenberger: Funding acquisition, Resources, Supervision, Validation, Writing: Original Draft Preparation; Ute Jungwirth: Formal Analysis, Funding acquisition, Resources, Supervision, Validation, Visualization, Writing: Original Draft Preparation, Writing: Review & Editing; Gernot Walko: Conceptualization, Data Curation, Formal Analysis, Funding acquisition, Methodology, Project Administration, Resources, Supervision, Validation, Visualization, Writing: Original Draft Preparation, Writing: Review &Editing.

Data availability

The authors declare that all data supporting the findings of this study are available within the paper and its supplementary information files. Raw Illumina sequencing data have been deposited in the Gene Expression Omnibus (GEO) following the MIAME guidelines, under the accession number GSE284725. The mass spectrometry proteomics data have been deposited to the ProteomeXchange Consortium via the PRIDE partner repository with the dataset identifier PXD061022 and 10.6019/PXD061022. DNAscent data have been deposited on European Nucleotide Archive (ENA), accession ID PRJEB103830.

References

1 Dotto GP, Rustgi AK. Squamous Cell Cancers: A Unified Perspective on Biology and Genetics. *Cancer Cell* 2016; 29: 622-637.

2 Winge MCG, Kellman LN, Guo K, Tang JY, Swetter SM, Aasi SZ *et al*. Advances in cutaneous squamous cell carcinoma. *Nat Rev Cancer* 2023; 23: 430-449.

3 da Costa A, Chowdhury D, Shapiro GI, D'Andrea AD, Konstantinopoulos PA. Targeting replication stress in cancer therapy. *Nat Rev Drug Discov* 2023; 22: 38-58.

4 Gaillard H, Garcia-Muse T, Aguilera A. Replication stress and cancer. *Nat Rev Cancer* 2015; 15: 276-289.

5 Bowry A, Kelly RDW, Petermann E. Hypertranscription and replication stress in cancer. *Trends Cancer* 2021; 7: 863-877.

6 Molinuevo R, Freije A, Contreras L, Sanz JR, Gandarillas A. The DNA damage response links human squamous proliferation with differentiation. *J Cell Biol* 2020; 219.

7 Freije A, Ceballos L, Coisy M, Barnes L, Rosa M, De Diego E *et al*. Cyclin E drives human keratinocyte growth into differentiation. *Oncogene* 2012; 31: 5180-5192.

8 Freije A, Molinuevo R, Ceballos L, Cagigas M, Alonso-Lecue P, Rodriguez R *et al*. Inactivation of p53 in Human Keratinocytes Leads to Squamous Differentiation and Shedding via Replication Stress and Mitotic Slippage. *Cell Rep* 2014; 9: 1349-1360.

9 Gandarillas A, Davies D, Blanchard JM. Normal and c-Myc-promoted human keratinocyte differentiation both occur via a novel cell cycle involving cellular growth and endoreplication. *Oncogene* 2000; 19: 3278-3289.

10 Alonso-Lecue P, de Pedro I, Coulon V, Molinuevo R, Lorz C, Segrelles C *et al*. Inefficient differentiation response to cell cycle stress leads to genomic instability and malignant progression of squamous carcinoma cells. *Cell Death Dis* 2017; 8: e2901.

11 Blasiak J, Szczepanska J, Sobczuk A, Fila M, Pawlowska E. RIF1 Links Replication Timing with Fork Reactivation and DNA Double-Strand Break Repair. *Int J Mol Sci* 2021; 22.

12 Foti R, Gnan S, Cornacchia D, Dileep V, Bulut-Karslioglu A, Diehl S *et al*. Nuclear Architecture Organized by Rif1 Underpins the Replication-Timing Program. *Mol Cell* 2016; 61: 260-273.

13 Gnan S, Flyamer IM, Klein KN, Castelli E, Rapp A, Maiser A *et al*. Nuclear organisation and replication timing are coupled through RIF1-PP1 interaction. *Nat Commun* 2021; 12: 2910.

14 Moriyama K, Yoshizawa-Sugata N, Masai H. Oligomer formation and G-quadruplex binding by purified murine Rif1 protein, a key organizer of higher-order chromatin architecture. *J Biol Chem* 2018; 293: 3607-3624.

15 Cornacchia D, Dileep V, Quivy JP, Foti R, Tili F, Santarella-Mellwig R *et al*. Mouse Rif1 is a key regulator of the replication-timing programme in mammalian cells. *EMBO J* 2012; 31: 3678-3690.

16 Alver RC, Chadha GS, Gillespie PJ, Blow JJ. Reversal of DDK-Mediated MCM Phosphorylation by Rif1-PP1 Regulates Replication Initiation and Replisome Stability Independently of ATR/Chk1. *Cell Rep* 2017; 18: 2508-2520.

17 Moiseeva TN, Yin Y, Calderon MJ, Qian C, Schamus-Haynes S, Sugitani N *et al*. An ATR and CHK1 kinase signaling mechanism that limits origin firing during unperturbed DNA replication. *Proc Natl Acad Sci U S A* 2019; 116: 13374-13383.

18 Yamazaki S, Ishii A, Kanoh Y, Oda M, Nishito Y, Masai H. Rif1 regulates the replication timing domains on the human genome. *EMBO J* 2012; 31: 3667-3677.

19 Hiraga SI, Ly T, Garzon J, Horejsi Z, Ohkubo YN, Endo A *et al*. Human RIF1 and protein phosphatase 1 stimulate DNA replication origin licensing but suppress origin activation. *EMBO Rep* 2017; 18: 403-419.

20 Buonomo SB, Wu Y, Ferguson D, de Lange T. Mammalian Rif1 contributes to replication stress survival and homology-directed repair. *J Cell Biol* 2009; 187: 385-398.

21 Mukherjee C, Tripathi V, Manolika EM, Heijink AM, Ricci G, Merzouk S *et al*. RIF1 promotes replication fork protection and efficient restart to maintain genome stability. *Nat Commun* 2019; 10: 3287.

22 Garzon J, Ursich S, Lopes M, Hiraga SI, Donaldson AD. Human RIF1-Protein Phosphatase 1 Prevents Degradation and Breakage of Nascent DNA on Replication Stalling. *Cell Rep* 2019; 27: 2558-2566 e2554.

23 Dong Q, Day M, Saito Y, Parker E, Watts LP, Kanemaki MT *et al*. The human RIF1-Long isoform interacts with BRCA1 to promote recombinational fork repair under DNA replication stress. *Nat Commun* 2025; 16: 5820.

24 Wang H, Zhao A, Chen L, Zhong X, Liao J, Gao M *et al*. Human RIF1 encodes an anti-apoptotic factor required for DNA repair. *Carcinogenesis* 2009; 30: 1314-1319.

25 Eke I, Zong D, Aryankalayil MJ, Sandfort V, Bylicky MA, Rath BH *et al*. 53BP1/RIF1 signaling promotes cell survival after multifractionated radiotherapy. *Nucleic Acids Res* 2020; 48: 1314-1326.

26 Mei Y, Peng C, Liu YB, Wang J, Zhou HH. Silencing RIF1 decreases cell growth, migration and increases cisplatin sensitivity of human cervical cancer cells. *Oncotarget* 2017; 8: 107044-107051.

27 Noordermeer SM, Adam S, Setiaputra D, Barazas M, Pettitt SJ, Ling AK *et al*. The shieldin complex mediates 53BP1-dependent DNA repair. *Nature* 2018; 560: 117-121.

28 Franklin JM, Wu Z, Guan KL. Insights into recent findings and clinical application of YAP and TAZ in cancer. *Nat Rev Cancer* 2023; 23: 512-525.

29 Howard A, Bojko J, Flynn B, Bowen S, Jungwirth U, Walko G. Targeting the Hippo/YAP/TAZ signalling pathway: Novel opportunities for therapeutic interventions into skin cancers. *Exp Dermatol* 2022; 31: 1477-1499.

30 Maehama T, Nishio M, Otani J, Mak TW, Suzuki A. The role of Hippo-YAP signaling in squamous cell carcinomas. *Cancer Sci* 2021; 112: 51-60.

31 Hillmer RE, Link BA. The Roles of Hippo Signaling Transducers Yap and Taz in Chromatin Remodeling. *Cells* 2019; 8.

32 Walko G, Woodhouse S, Pisco AO, Rognoni E, Liakath-Ali K, Lichtenberger BM *et al*. A genome-wide screen identifies YAP/WBP2 interplay conferring growth advantage on human epidermal stem cells. *Nat Commun* 2017; 8: 14744.

33 De Rosa L, Secone Seconetti A, De Santis G, Pellacani G, Hirsch T, Rothoeft T *et al*. Laminin 332-Dependent YAP Dysregulation Depletes Epidermal Stem Cells in Junctional Epidermolysis Bullosa. *Cell Rep* 2019; 27: 2036-2049 e2036.

34 Lavado A, Park JY, Pare J, Finkelstein D, Pan H, Xu B *et al*. The Hippo Pathway Prevents YAP/TAZ-Driven Hypertranscription and Controls Neural Progenitor Number. *Dev Cell* 2018; 47: 576-591 e578.

35 Gertzmann D, Presek C, Mattes AL, Sanger M, Zoller M, Schulein-Volk C *et al*. Oncogenic YAP sensitizes cells to CHK1 inhibition via CDK4/6 driven G1 acceleration. *EMBO Rep* 2025.

36 Yuan Y, Park J, Feng A, Awasthi P, Wang Z, Chen Q *et al*. YAP1/TAZ-TEAD transcriptional networks maintain skin homeostasis by regulating cell proliferation and limiting KLF4 activity. *Nat Commun* 2020; 11: 1472.

37 Rheinwald JG, Beckett MA. Tumorigenic keratinocyte lines requiring anchorage and fibroblast support cultured from human squamous cell carcinomas. *Cancer Res* 1981; 41: 1657-1663.

38 Zanconato F, Forcato M, Battilana G, Azzolin L, Quaranta E, Bodega B *et al*. Genome-wide association between YAP/TAZ/TEAD and AP-1 at enhancers drives oncogenic growth. *Nat Cell Biol* 2015; 17: 1218-1227.

39 Pattschull G, Walz S, Grundl M, Schwab M, Ruhl E, Baluapuri A *et al*. The Myb-MuvB Complex Is Required for YAP-Dependent Transcription of Mitotic Genes. *Cell Rep* 2019; 27: 3533-3546 e3537.

40 Lopez-Pajares V, Qu K, Zhang J, Webster DE, Barajas BC, Siprashvili Z *et al*. A LncRNA-MAF:MAFB transcription factor network regulates epidermal differentiation. *Dev Cell* 2015; 32: 693-706.

41 Kypriotou M, Huber M, Hohl D. The human epidermal differentiation complex: cornified envelope precursors, S100 proteins and the 'fused genes' family. *Exp Dermatol* 2012; 21: 643-649.

42 Wang J, Harwood CA, Bailey E, Bewicke-Copley F, Anene CA, Thomson J *et al*. Transcriptomic analysis of cutaneous squamous cell carcinoma reveals a multigene prognostic signature associated with metastasis. *J Am Acad Dermatol* 2023; 89: 1159-1166.

43 Hagenbeek TJ, Zbieg JR, Hafner M, Mroue R, Lacap JA, Sodir NM *et al*. An allosteric pan-TEAD inhibitor blocks oncogenic YAP/TAZ signaling and overcomes KRAS G12C inhibitor resistance. *Nat Cancer* 2023; 4: 812-828.

44 Yuan Y, Salinas Parra N, Chen Q, Iglesias-Bartolome R. Oncogenic Hedgehog-smoothened signaling depends on YAP1-TAZ/TEAD transcription to restrain differentiation in basal cell carcinoma. *J Invest Dermatol* 2021.

45 Ashley AK, Shrivastav M, Nie J, Amerin C, Troksa K, Glanzer JG *et al*. DNA-PK phosphorylation of RPA32 Ser4/Ser8 regulates replication stress checkpoint activation, fork restart, homologous recombination and mitotic catastrophe. *DNA Repair (Amst)* 2014; 21: 131-139.

46 Liu S, Opiyo SO, Manthey K, Glanzer JG, Ashley AK, Amerin C *et al*. Distinct roles for DNA-PK, ATM and ATR in RPA phosphorylation and checkpoint activation in response to replication stress. *Nucleic Acids Res* 2012; 40: 10780-10794.

47 Dempster JM, Pacini C, Pantel S, Behan FM, Green T, Krill-Burger J *et al*. Agreement between two large pan-cancer CRISPR-Cas9 gene dependency data sets. *Nat Commun* 2019; 10: 5817.

48 Takahashi N, Kim S, Schultz CW, Rajapakse VN, Zhang Y, Redon CE *et al*. Replication stress defines distinct molecular subtypes across cancers. *Cancer Res Commun* 2022; 2: 503-517.

49 Kotsantis P, Silva LM, Irmscher S, Jones RM, Folkes L, Gromak N *et al*. Increased global transcription activity as a mechanism of replication stress in cancer. *Nat Commun* 2016; 7: 13087.

50 Mohammed H, Taylor C, Brown GD, Papachristou EK, Carroll JS, D'Santos CS. Rapid immunoprecipitation mass spectrometry of endogenous proteins (RIME) for analysis of chromatin complexes. *Nat Protoc* 2016; 11: 316-326.

51 Zhang N, Bai H, David KK, Dong J, Zheng Y, Cai J *et al*. The Merlin/NF2 tumor suppressor functions through the YAP oncoprotein to regulate tissue homeostasis in mammals. *Dev Cell* 2010; 19: 27-38.

52 Zhou Y, Zhang J, Li H, Huang T, Wong CC, Wu F *et al*. AMOTL1 enhances YAP1 stability and promotes YAP1-driven gastric oncogenesis. *Oncogene* 2020; 39: 4375-4389.

53 Wang P, Bai Y, Song B, Wang Y, Liu D, Lai Y *et al*. PP1A-mediated dephosphorylation positively regulates YAP2 activity. *PLoS One* 2011; 6: e24288.

54 Zhu M, Peng R, Liang X, Lan Z, Tang M, Hou P *et al*. P4HA2-induced prolyl hydroxylation suppresses YAP1-mediated prostate cancer cell migration, invasion, and metastasis. *Oncogene* 2021; 40: 6049-6056.

55 Mittal P, Roberts CWM. The SWI/SNF complex in cancer - biology, biomarkers and therapy. *Nat Rev Clin Oncol* 2020; 17: 435-448.

56 He L, Pratt H, Gao M, Wei F, Weng Z, Struhl K. YAP and TAZ are transcriptional co-activators of AP-1 proteins and STAT3 during breast cellular transformation. *Elife* 2021; 10.

57 Ning B, Tilston-Lunel AM, Simonetti J, Hicks-Berthet J, Matschulat A, Pfefferkorn R *et al*. Convergence of YAP/TAZ, TEAD and TP63 activity is associated with bronchial premalignant severity and progression. *J Exp Clin Cancer Res* 2023; 42: 116.

58 Nowak DE, Tian B, Brasier AR. Two-step cross-linking method for identification of NF-kappaB gene network by chromatin immunoprecipitation. *Biotechniques* 2005; 39: 715-725.

59 Melendez Garcia R, Haccard O, Chesneau A, Narassimprakash H, Roger J, Perron M *et al*. A non-transcriptional function of Yap regulates the DNA replication program in Xenopus laevis. *Elife* 2022; 11.

60 Proby CM, Purdie KJ, Sexton CJ, Purkis P, Navsaria HA, Stables JN *et al*. Spontaneous keratinocyte cell lines representing early and advanced stages of malignant transformation of the epidermis. *Exp Dermatol* 2000; 9: 104-117.

61 Chandrashekar DS, Karthikeyan SK, Korla PK, Patel H, Shovon AR, Athar M *et al*. UALCAN: An update to the integrated cancer data analysis platform. *Neoplasia* 2022; 25: 18-27.

62 Zhang Y, Chen F, Chandrashekar DS, Varambally S, Creighton CJ. Proteogenomic characterization of 2002 human cancers reveals pan-cancer molecular subtypes and associated pathways. *Nat Commun* 2022; 13: 2669.

63 Jones MJK, Rai SK, Pfuderer PL, Bonfim-Melo A, Pagan JK, Clarke PR *et al*. A high-resolution, nanopore-based artificial intelligence assay for DNA replication stress in human cancer cells. *Nat Commun* 2025; 16: 7732.

64 Maya-Mendoza A, Moudry P, Merchut-Maya JM, Lee M, Strauss R, Bartek J. High speed of fork progression induces DNA replication stress and genomic instability. *Nature* 2018; 559: 279-284.

65 Raso MC, Djoric N, Walser F, Hess S, Schmid FM, Burger S *et al*. Interferon-stimulated gene 15 accelerates replication fork progression inducing chromosomal breakage. *J Cell Biol* 2020; 219.

66 Fousek-Schuller VJ, Borgstahl GEO. The Intriguing Mystery of RPA Phosphorylation in DNA Double-Strand Break Repair. *Genes (Basel)* 2024; 15.

67 Toledo LI, Altmeyer M, Rask MB, Lukas C, Larsen DH, Povlsen LK *et al*. ATR prohibits replication catastrophe by preventing global exhaustion of RPA. *Cell* 2013; 155: 1088-1103.

68 Picco G, Chen ED, Alonso LG, Behan FM, Goncalves E, Bignell G *et al*. Functional linkage of gene fusions to cancer cell fitness assessed by pharmacological and CRISPR-Cas9 screening. *Nat Commun* 2019; 10: 2198.

69 Petermann E, Orta ML, Issaeva N, Schultz N, Helleday T. Hydroxyurea-stalled replication forks become progressively inactivated and require two different RAD51-mediated pathways for restart and repair. *Mol Cell* 2010; 37: 492-502.

70 Moeglin E, Desplancq D, Conic S, Oulad-Abdelghani M, Stoessel A, Chiper M *et al*. Uniform Widespread Nuclear Phosphorylation of Histone H2AX Is an Indicator of Lethal DNA Replication Stress. *Cancers (Basel)* 2019; 11.

71 Cui P, Lin Q, Xin C, Han L, An L, Wang Y *et al*. Hydroxyurea-induced global transcriptional suppression in mouse ES cells. *Carcinogenesis* 2010; 31: 1661-1668.

72 Li Q, Tie Y, Alu A, Ma X, Shi H. Targeted therapy for head and neck cancer: signaling pathways and clinical studies. *Signal Transduct Target Ther* 2023; 8: 31.

73 Sato K, Faraji F, Cervantes-Villagrana RD, Wu X, Koshizuka K, Ishikawa T *et al*. Targeting YAP/TAZ-TEAD signaling as a therapeutic approach in head and neck squamous cell carcinoma. *Cancer Lett* 2025: 217467.

74 Chang CY, Shipony Z, Lin SG, Kuo A, Xiong X, Loh KM *et al*. Increased ACTL6A occupancy within mSWI/SNF chromatin remodelers drives human squamous cell carcinoma. *Mol Cell* 2021; 81: 4964-4978 e4968.

75 Kim M, Kim T, Johnson RL, Lim DS. Transcriptional co-repressor function of the hippo pathway transducers YAP and TAZ. *Cell Rep* 2015; 11: 270-282.

76 Debaugnies M, Sanchez-Danes A, Rorive S, Raphael M, Liagre M, Parent MA *et al*. YAP and TAZ are essential for basal and squamous cell carcinoma initiation. *EMBO Rep* 2018.

77 Inman GJ, Wang J, Nagano A, Alexandrov LB, Purdie KJ, Taylor RG *et al*. The genomic landscape of cutaneous SCC reveals drivers and a novel azathioprine associated mutational signature. *Nat Commun* 2018; 9: 3667.

78 Pennycook BR, Vesela E, Peripolli S, Singh T, Barr AR, Bertoli C *et al*. E2F-dependent transcription determines replication capacity and S phase length. *Nat Commun* 2020; 11: 3503.

79 Kumagai A, Dunphy WG. Binding of the Treslin-MTBP Complex to Specific Regions of the Human Genome Promotes the Initiation of DNA Replication. *Cell Rep* 2020; 32: 108178.

80 Watts LP, Natsume T, Saito Y, Garzon J, Dong Q, Boteva L *et al*. The RIF1-long splice variant promotes G1 phase 53BP1 nuclear bodies to protect against replication stress. *Elife* 2020; 9.

Figure legends

Figure 1. YAP/TAZ-TEAD-mediated oncogenic transcriptional programmes control the balance between proliferation and differentiation in squamous cell carcinoma progression.

(**A**, **B**) Violin blots (thick line, median; thin lines, upper- and lower quartiles) show the distribution of Gene Set Variation Analysis (GSVA) scores for differentially expressed genes

835 (DEGs) that were (A) downregulated or (B) upregulated in siYAP/TAZ SCC13 cells across
836 different cSCC patient samples [42]. Norm_no_met / Tum_no_met: perilesional normal skin
837 and primary cSCC tissue from patients with no metastasis over 3 years; Norm_with_met /
838 Tum_with_met: perilesional normal skin and primary cSCC tissue from patients with
839 metastasis during 3 years follow-up; Met: tissue from metastasis. Pairwise comparisons
840 between sample groups were conducted using a *t* test. The p-values from these comparisons
841 are indicated above the boxplots with brackets linking the compared groups. The
842 significance levels are denoted as follows: *p=0.032; **p=0.0021; ***p=0.0002;
843 ****p<0.0001. (**C**) Photograph shows lack of medium acidification by doxycycline-induced
844 shYAP compared to shNTC SCC13 cells during a 4-day culture period. (**D**) Immunoblot
845 analysis of SCC13 cells expressing doxycycline-induced shYAP, shTAZ, or shNTC for 72 h, using
846 the indicated antibodies. Actin or cyclophilin B (CBP) were used as loading controls. (**E**) Cell
847 cycle analysis by propidium iodide (PI) labelling of asynchronous populations of shNTC and
848 shYAP SCC13 cells (grey profiles), and of cells synchronised at the G1/S boundary by double
849 thymidine block (dTb) and released into S phase and analysed at indicated time points
850 (T=hours post thymidine release, coloured profiles). (**F**) Colony formation assays were
851 quantified by measuring the percentage of well area occupied by colonies. Bars show the
852 means from n=3 independent experiments (performed with 3 technical replicates),
853 individual data points (different shapes indicate different experiments) show the means
854 from each experiment, error bars show SD. Exact p-values are shown, RM one way ANOVA
855 with Geisser-Greenhouse correction and Dunnett's multiple comparison test. (**G**) 3D
856 spheroid growth of shNTC and shYAP SCC13 cells. p-values are shown for multiple
857 comparisons at all timepoints, Ordinary two-way ANOVA and Šidák's multiple comparison

858 test. *p<0.033, **p<0.002, ***p<0.001. Sources of variation: shRNA, p<0.001; time,
859 p<0.001; shRNA x time, p<0.001.
860
861 ***Figure 2.*** **Pharmacological inhibition of YAP/TAZ-TEAD complex formation phenocopies YAP**
862 **depletion.**
863 (**A**) Representative proliferation dose–response curves (means±SD) of SCC13 cells treated
864 with different TEAD inhibitors. (**B**) Representative viability dose–response curves
865 (means±SD) of different cell lines from a human cSCC progression series [60] treated with
866 different GNE-7883 concentrations. (**C**) Immunoblot analysis of SCC13 cells treated with
867 vehicle control (DMSO) or GNE-7883 (2 µM) for 48 h, using the indicated antibodies. Tubulin
868 was used as loading control. (**D**) qRT-PCR analysis of *IVL* mRNA expression in SCC13 cells
869 treated with GNE-7883 (2 µM). Data shown are from n=1 experiment performed with three
870 technical replicates. Individual data points: mean fold change in mRNA abundance
871 (normalized to GAPDH) compared to DMSO control. Bars represent the means from all
872 replicates; error bars represent SD. (**E**) SCC13 3D spheroid growth in the presence of vehicle
873 (DMSO) or different concentrations of GNE-7883 (GNE). p-values are shown for multiple
874 comparisons at 12 days timepoint, Ordinary two-way ANOVA and Dunnett's multiple
875 comparison test. *p<0.033, **p<0.002, ***p<0.001. Sources of variation: GNE treatment,
876 p<0.001; time, p<0.001; GNE treatment x time, p<0.001. (**F**) Cell viability measured at the
877 endpoint of the experiment shown in (E). Each datapoint represents one spheroid. Bars
878 represent the means from all spheroids; error bars represent SD. Exact p-values are shown,
879 Kruskal-Wallis test with Dunn's multiple comparison test. (**G**) Immunoblot analysis of SCC13
880 cells expressing shNTC or different shP21 treated with vehicle control (DMSO) or GNE-7883
881 (2 µM), using the indicated antibodies. Tubulin was used as loading control. (**H**) Phase

882 contrast images show that p21 depletion rescues cell viability in GNE-7883 (2 µM)-treated
883 SCC13 cells. Bar, 10 µm.
884
885 ***Figure 3. RIME identifies RIF1 as an interactor of chromatin-associated YAP in squamous***
886 ***cell carcinoma cells.***
887 (**A**) Interaction network of YAP protein interactors identified by RIME in SCC13 cells. Oval
888 nodes: proteins that were previously identified as candidate regulators of SCC13 cell
889 proliferation and/or survival in a genome wide RNA-interference (RNAi) screen (hit:
890 'Yes')[32]; rectangular shaped nodes: proteins that were not identified in the RNAi screen
891 (hit: 'No'). Red connecting lines (edges) show previously identified YAP interactions
892 according to the STRING Homo sapiens database, and nodes with red borders indicate
893 known YAP interactors (manually curated from STRING and literature search); dashed red
894 lines show manually curated known YAP interactions that were not yet present in the
895 STRING database. Proteins were manually grouped based on function (gene names
896 displayed, generated in Cytoscape 3.9.1 using STRING app 1.7.1). (**B**) Gene ontology terms
897 ('molecular functions' and 'biological process') enriched within the high-confidence YAP-
898 interacting proteins identified by RIME. (**C**) Confocal fluorescence image (z-projection) of YAP
899 (green) and RIF1 (red) nuclear localisation in SCC13 cells. DNA was counterstained with
900 Hoechst dye (blue). Scale bar, 10 µm. (**D**, **E**) Immunoblot analysis of YAP and IgG-control
901 immunoprecipitates and respective inputs from SCC13 (D) whole cell extracts and (E) and
902 nuclei-enriched fractions using the indicated antibodies. (**F**, **G**) Representative confocal
903 microscopy images (z-projections) and image quantifications of (F) YAP-RIF1 and (G) YAP-
904 TEAD1 in-situ PLA in control (siNTC&shNTC) and YAP/TAZ knockdown (siYAP/TAZ&shYAP)
905 cells (PLA signal, green; DNA (DAPI) blue; n >250 cells (YAP-RIF1), n >500 cells (YAP-TEAD1)

906 per condition in n=3 independent experiments). Scale bars, 5 µm. Datapoints show fold
907 decrease in mean nuclear PLA signal intensity in siYAP/TAZ&shYAP cells compared to
908 siNTC&shNTC cells. Lines show means from all three experiments, error bars show SD. Exact
909 p-values are shown, one sample two-tailed *t* test.
910
911 ***Figure 4. YAP/TAZ-TEAD modulate RIF1 protein stability.***
912 (**A**) qRT-PCR analysis of *RIF1* mRNA expression in SCC13 cells transfected with an siRNA
913 SMARTpool targeting YAP/TAZ (siY/T) or a non-targeting control SMARTpool (siNTC) for 48 h.
914 Data shown are from n=3 independent experiments performed with three technical
915 replicates. Individual data points: mean fold change in mRNA abundance (normalized to
916 GAPDH) compared to siNTC in each experiment. Bars represent the means from all
917 experiments, error bars represent SD. Exact p-values are shown, paired *t* test. (**B–D**)
918 Immunoblot analysis of SCC13 cells (B) transfected with siNTC or siY/T for 48 h, (C)
919 expressing empty vector control (MCS) or different YAP transgenes upon doxycycline (dox)
920 induction, or (D) treated with GNE-7883 (2 µM) for 24 h, using the indicated antibodies.
921 Tubulin or cyclophilin B (CBP) were used as loading controls. Arrows, position of full-length
922 RIF1 bands. In (B, D) numbers below lanes represent protein ratios relative to an arbitrary
923 level of 1.0 set for siNTC or DMSO control, respectively. (**E**) qRT-PCR analysis of *RIF1* mRNA
924 expression in SCC13 cells treated with GNE-7883 for 24 h. Data shown are from n=1
925 experiment performed with three technical replicates. Individual data points: mean fold
926 change in mRNA abundance (normalized to GAPDH) compared to DMSO control. Bars
927 represent the means from all replicates, error bars represent SD. (**F**) Immunoblot analysis of
928 RIF1 protein levels in SCC13 cells transfected with siRNA SMARTpools targeting TEAD1,
929 TEAD3, TEAD4, or YAP/TAZ (siY/T), or an siNTC SMARTpool for 24 h. Cyclophilin B (CBP) was

930 used as loading control. (**G**) Quantification of RIF1 protein expression in experiment shown
931 in (F). Individual data points show fold change in RIF1 protein levels (normalised to tubulin)
932 in siTEAD1, siTEAD3, siTEAD4, siTEAD1/3/4, and siY/T compared to siNTC in n=3 independent
933 experiments (different shapes of data points), bars show the mean, error bars show SD. (**H**)
934 Immunoblot analysis of chromatin fractions from SCC13 cells expressing doxycycline-induced
935 shYAP or shNTC for 48 h, using the indicated antibodies. Cells were synchronised at the G1/S
936 boundary by double thymidine block (dTb) and released into the S phase. Histone H3 (HH3)
937 was used as loading control. Arrow, position of full-length RIF1 band. (**I**) Quantification of
938 RIF1 protein levels in experiment shown in (H). Individual data points show fold change in
939 RIF1 protein levels (normalised to HH3) compared to shNTC at timepoint 0 h in n=2
940 independent experiments (different shapes of data points).
941
942 ***Figure 5. Increased expression of RIF1 in squamous cell carcinoma.***
943 (**A**) Immunoblot analysis of normal human epidermal keratinocytes (NHKs), keratinocytes
944 isolated from a pre-malignant dysplastic skin lesion (PM1), various cell lines isolated from
945 primary cutaneous SCCs (cSCC; SCC13, SCC-NR, MET1), a recurrent cSCC (MET2), and a
946 lymph node metastasis (MET4), using the indicated antibodies. Actin was used as loading
947 control. Arrow, position of full-length RIF1 band. (**B**, **C**) Quantification (B) and representative
948 images (C) of RIF1 expression in healthy adult human skin (HS), nodular (Nod) and (Inf)
949 infiltrative basal cell carcinoma (BCC), and well-differentiated (WD) and poorly differentiated
950 (PD) cSCC. Tissue sections were immunolabelled with antibodies against RIF1 (green), and
951 keratin 14 (Krt14, blue) to identify normal and neoplastic epidermal keratinocytes. White
952 dotted line demarcates dermal–epidermal boundary in HS. Scale bar, 50 µm. Superplots in
953 (B) show percentage of RIF1-positive keratinocytes in different areas of the same tumour

954 (coloured symbols), mean percentage of RIF1-positive keratinocytes in 3–5 different patient
955 samples (black datapoints), and mean percentage of RIF1-positive keratinocytes in each
956 sample group (lines). Error bars show SD from each sample group. *p<0.05, Brown-Forsythe
957 and Welsh ANOVA test with Dunett's multiple comparison test. (**D**, **E**) RIF1 protein
958 expression in HNSCC samples from the Clinical Proteomic Tumour Analysis Consortium
959 (CPTAC), stratified according to (D) tumour stage, or (E) presence of alterations in the Hippo
960 pathway or other signalling pathways. Jitter plots (overlayed onto box plots) show Z-values
961 (standard deviations from the median across samples for the given sample type) from
962 individual samples. Box plots indicate the median (middle line), 25th percentile (bottom line),
963 75th percentile (top line), and minimum and maximum (whiskers). Log2 spectral count ratio
964 values from CPTAC were first normalized within each sample profile, then normalized across
965 samples. Graphs were downloaded from the UALCAN database
966 (https://ualcan.path.uab.edu/). (D) p<0.05 for all pairwise comparisons. In (E) exact p-values
967 are shown.
968
969 ***Figure 6. Depletion of RIF1 in squamous cell carcinoma cells affects DNA replication***
970 ***dynamics.***
971 (**A**) Representative cell cycle analysis by PI labelling of asynchronous populations of shNTC
972 and shRIF1 SCC13 cells (grey profiles) and of cells synchronised at the G1/S boundary by
973 double thymidine block (dTb) and released into S phase (T=hours post thymidine release,
974 coloured profiles). (**B**, **C**) Immunoblot analysis of (B) cell extracts and (C) chromatin fractions
975 from shNTC and shRIF1 SCC13 cells, using the indicated antibodies. In (C) cells were
976 synchronised at the G1/S boundary by double thymidine block (dTB) and released into the S
977 phase. Note that DDK-induced phosphorylation of MCM4 results in a band shift. Cyclophilin

978 B (CPB), tubulin, and histone H3 (HH3) were used as loading controls. shRIF1-017 was used
979 in experiments shown in (A, C). Arrows in (B, C), position of full-length RIF1 band. (**D, E**)
980 Replication fork speed (D) and replication track length (E) measured by DNAscent. Mean fork
981 speed (kb/min) and track length (bp) are indicated. Black bars show medians. Total number
982 of forks scored in n=2 independent experiments: shNTC=5632; shRIF1=6216. (**F**) Combined
983 distribution of stall scores from n=2 independent experiments. Mean stall cores are
984 indicated.
985
986 ***Figure 7. RIF1 protects against endogenous replication stress.***
987 (**A, B**) Immunoblot analysis of cell extracts from SCC13 cells expressing shNTC or different
988 shRIF1, using the indicated antibodies. Cyclophilin B (CPB), tubulin, or GAPDH were used as
989 loading controls. Cells treated for 24 h with 4 mM HU served as positive controls for severe
990 replication stress. Positions of strongly hyperphosphorylated RPA32 bands are indicated with
991 asterisks. Arrows, positions of full-length RIF1 bands. (**C**) Representative cell cycle profile (PI
992 labelling following a 30-min EdU pulse) of unsynchronised shNTC and shRIF1 SCC13 cells.
993 Gates used for quantification of percentage of cells in the different cell cycle phases are
994 shown. (**D**) Quantification of percentage of cells in different cell cycle phases. Bars show
995 means from n=4 independent experiments, individual data points show cell percentages in
996 each experiment, error bars show SD. Exact p-values are shown, paired *t* test. (**E, F**)
997 Immunoblot analysis of cell extracts from SCC13 cells transfected with (E) siNTC, siYAP/TAZ
998 (siY/T), or siRIF1 for 48 h, or treated with cisplatin (CP, 4 µM) or hydroxyurea (HU, 4 mM) for
999 24 h to induce S phase arrest, or (F) expressing shNTC or different shRIF1, using the indicated
1000 antibodies. Tubulin was used as loading control. (**G**) Representative images of colony
1001 formation efficiency of shNTC and shRIF1 SCC13 cells. Cells in triplicate wells were stained

1002 with crystal violet. (**H**) Percentage of well area occupied by colonies. Bars show the means
1003 from n=3 independent experiments (performed with 3 technical replicates), individual data
1004 points (different shapes indicate different experiments) show the means from each
1005 experiment, error bars show SD. Exact p-values are shown, RM one way ANOVA with
1006 Geisser-Greenhouse correction and Dunnett's multiple comparison test.
1007
1008 ***Figure 8. YAP is involved in DNA damage repair at collapsed replication forks.***
1009 (**A**) Immunoblot analysis of SCC13 control cells and cells exposed to 4 mM hydroxyurea (HU)
1010 for 24 h, using the indicated antibodies. Washout, medium removal and replacement with
1011 fresh medium. Tubulin or cyclophilin B (CBP) were used as loading controls. (**B**)
1012 Representative microscopy images of RAD51 (green) foci in SCC13 cells treated with 4 mM
1013 HU for the indicated times. Dashed outlines indicate nuclear areas from DNA counterstain
1014 with DAPI. Scale bar, 25 µm. (**C**) Immunoblot analysis of SCC13 cells exposed to 4 mM HU for
1015 24 h, followed by HU washout, using the indicated antibodies. Tubulin was used as loading
1016 control. (**D**, **E**) Image quantifications of (D) YAP-RIF1 and (E) YAP-γH2AX in-situ PLA in SCC13
1017 cells treated with 4 mM HU for the indicated times. >200 cells were measured per
1018 experimental condition in n=3 independent experiments. Superplots show nuclear PLA
1019 signal intensity per cell (grey datapoints), mean nuclear PLA signal intensity of the respective
1020 cell populations in each of n=3 experiments (black datapoints, different shapes indicate
1021 different experiments), and mean nuclear PLA signal intensity from all three experiments
1022 (lines). Error bars show SD from all three experiments. Exact p-values are shown. (D) Brown-
1023 Forsythe and Welsh ANOVA test with Dunett's multiple comparison test, (E) unpaired *t* test.
1024 (**F**) Immunoblot analysis of SCC13 cells treated with 2 mM HU for 24 h or left untreated
1025 (control), 24 h after transfection with siNTC or siYAP/TAZ (siY/T), using the indicated

antibodies. Tubulin was used as loading control. (**G, H**) Synergism of YAP depletion (shYAP) and HU treatment on clonal colony growth was quantified by measuring the percentage of well area occupied by colonies after 10 days in culture. In (H) values have been normalized to controls (no HU treatment) for shYAP and shNTC. Bars show the means from n=3 independent experiments (performed with 3 technical replicates), individual data points show the means from each experiment, error bars show SD. p-values are shown for multiple comparisons, RM two-way ANOVA (matched values are spread across a row) and Šidak's multiple comparison test. *$p<0.033$, **$p<0.002$, ***$p<0.001$. Sources of variation in (G, H): HU concentration, $p<0.001$; shRNA, $p<0.001$; HU concentration x shRNA, $p<0.001$.

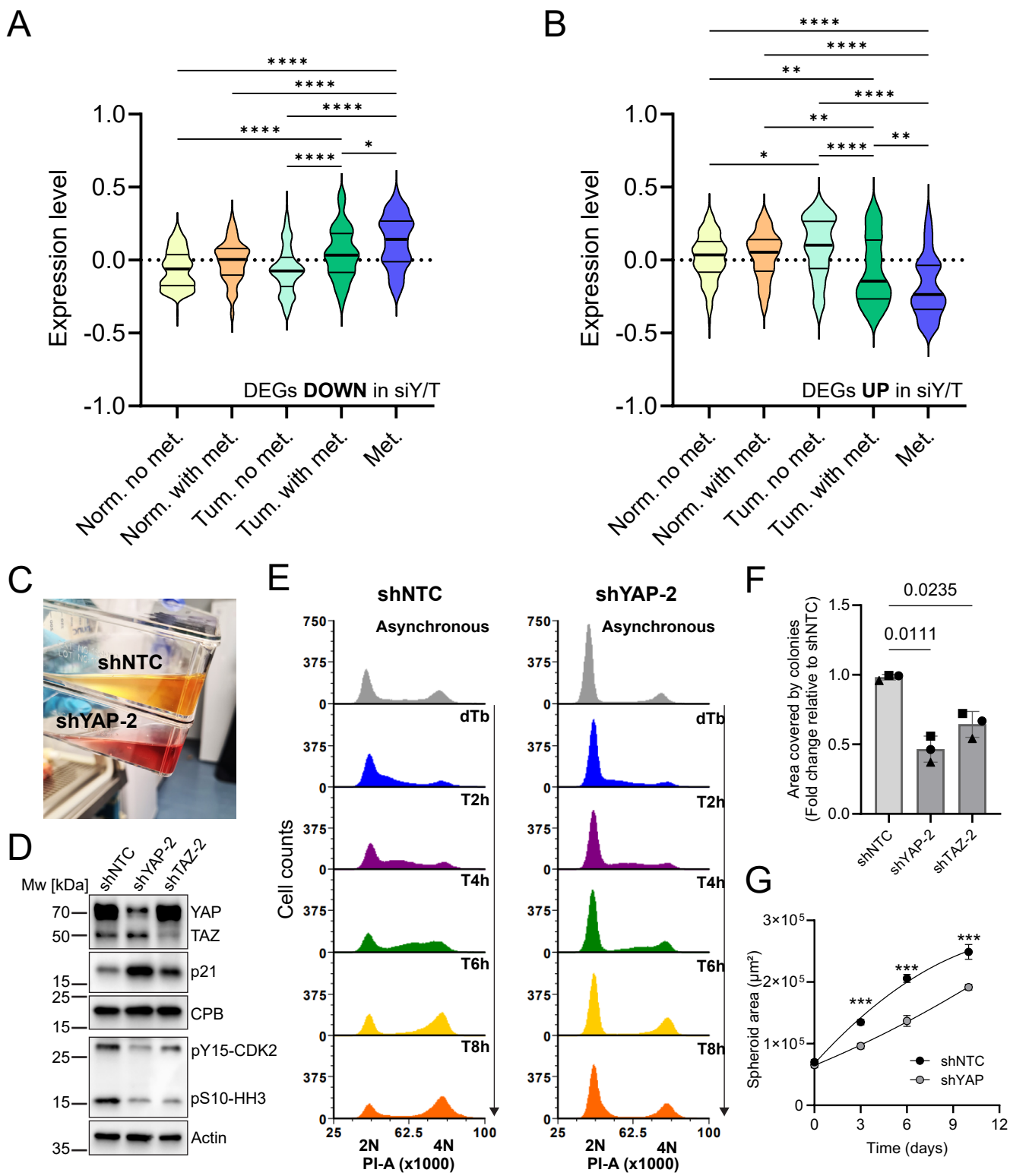

Figure 1_Bojko et al.

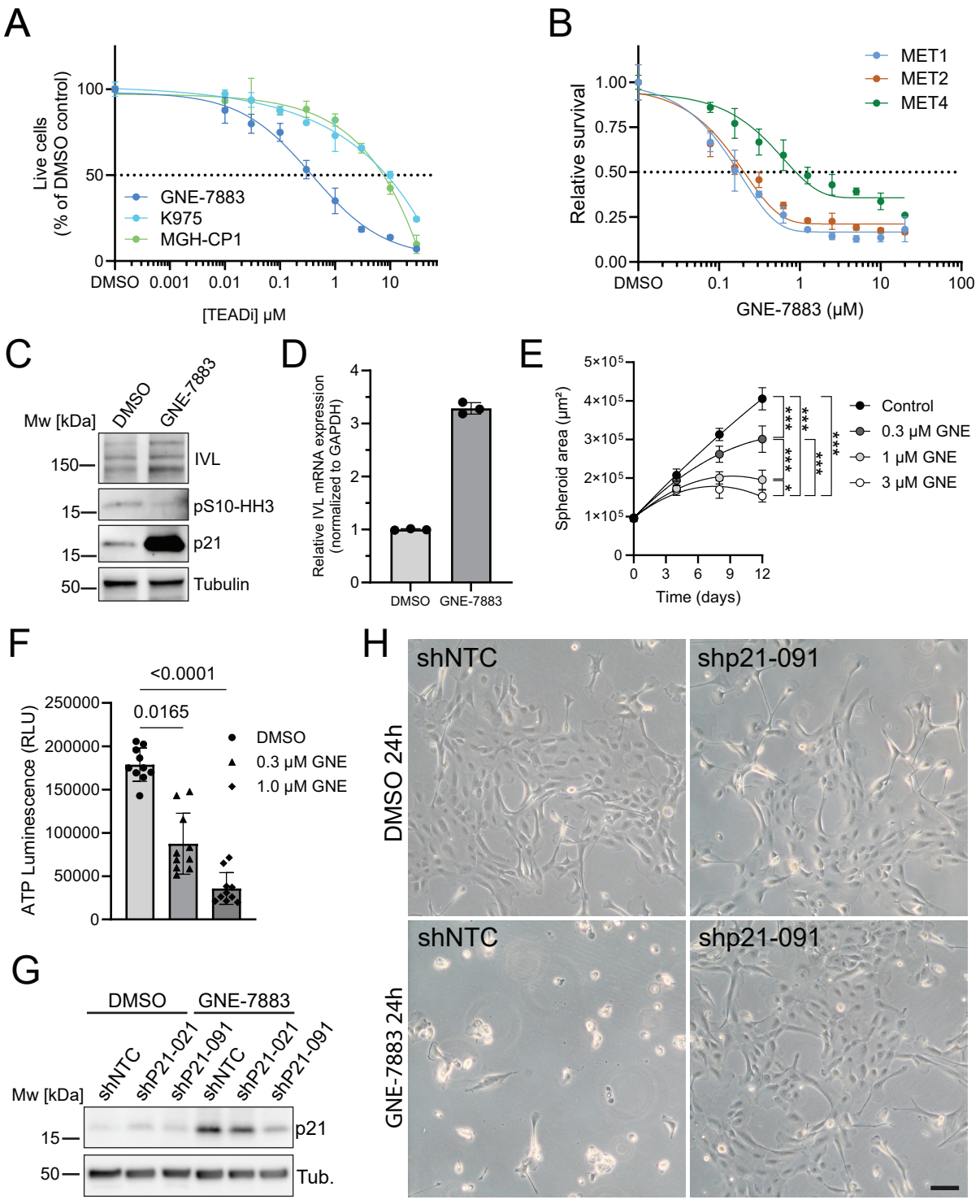

Figure 2_Bojko et al.

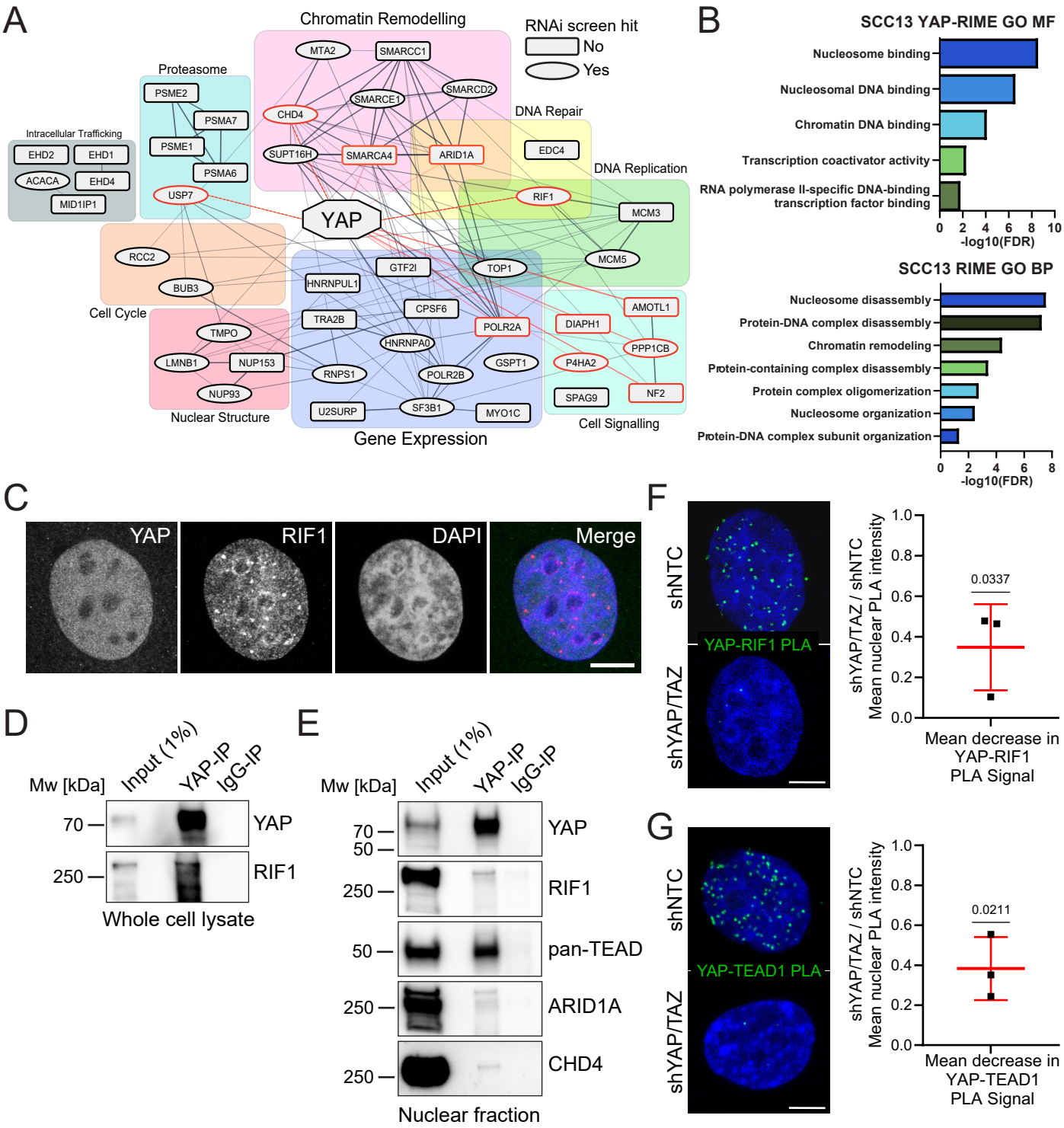

Figure 3_Bojko et al.

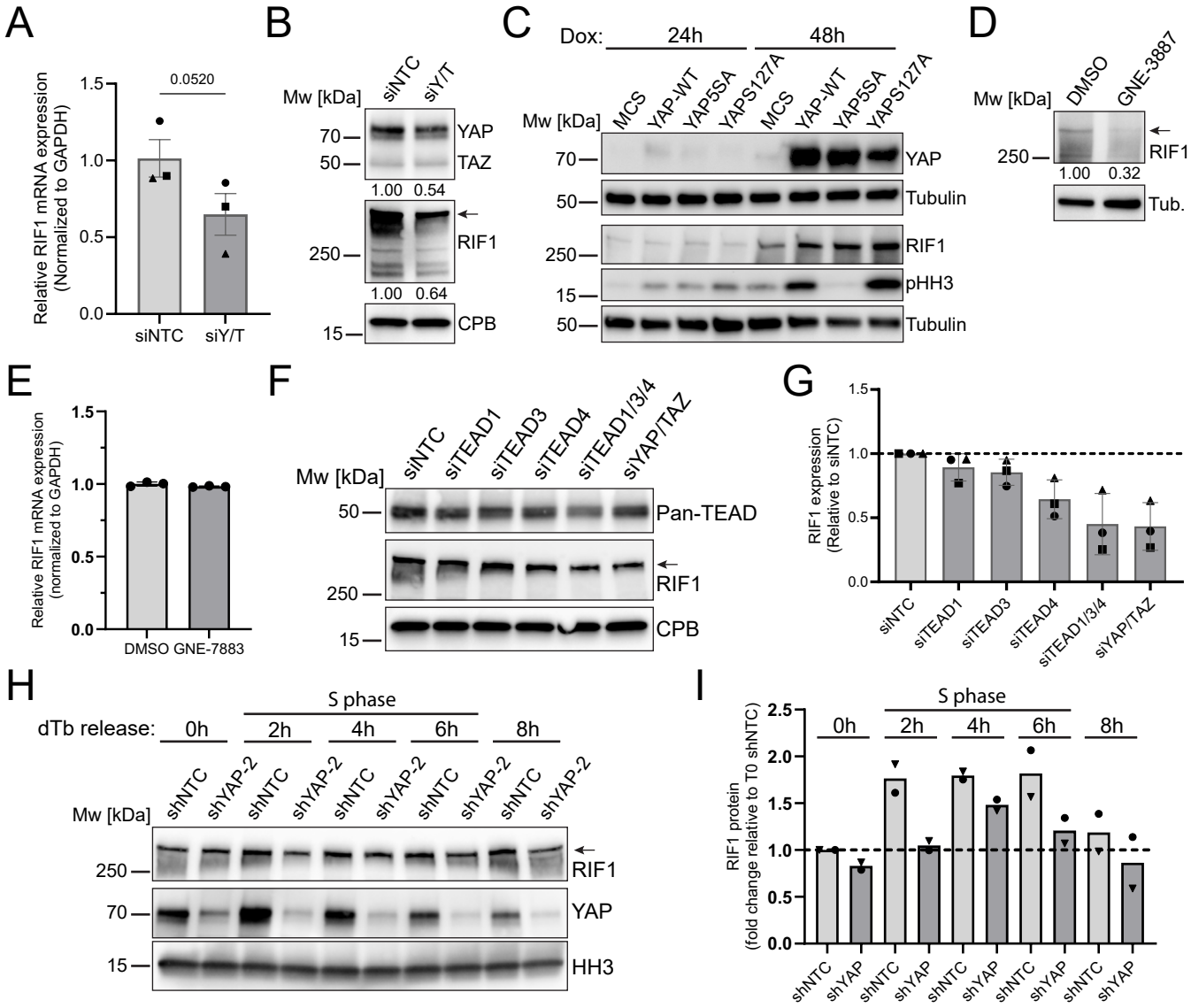

Figure 4_Bojko et al.

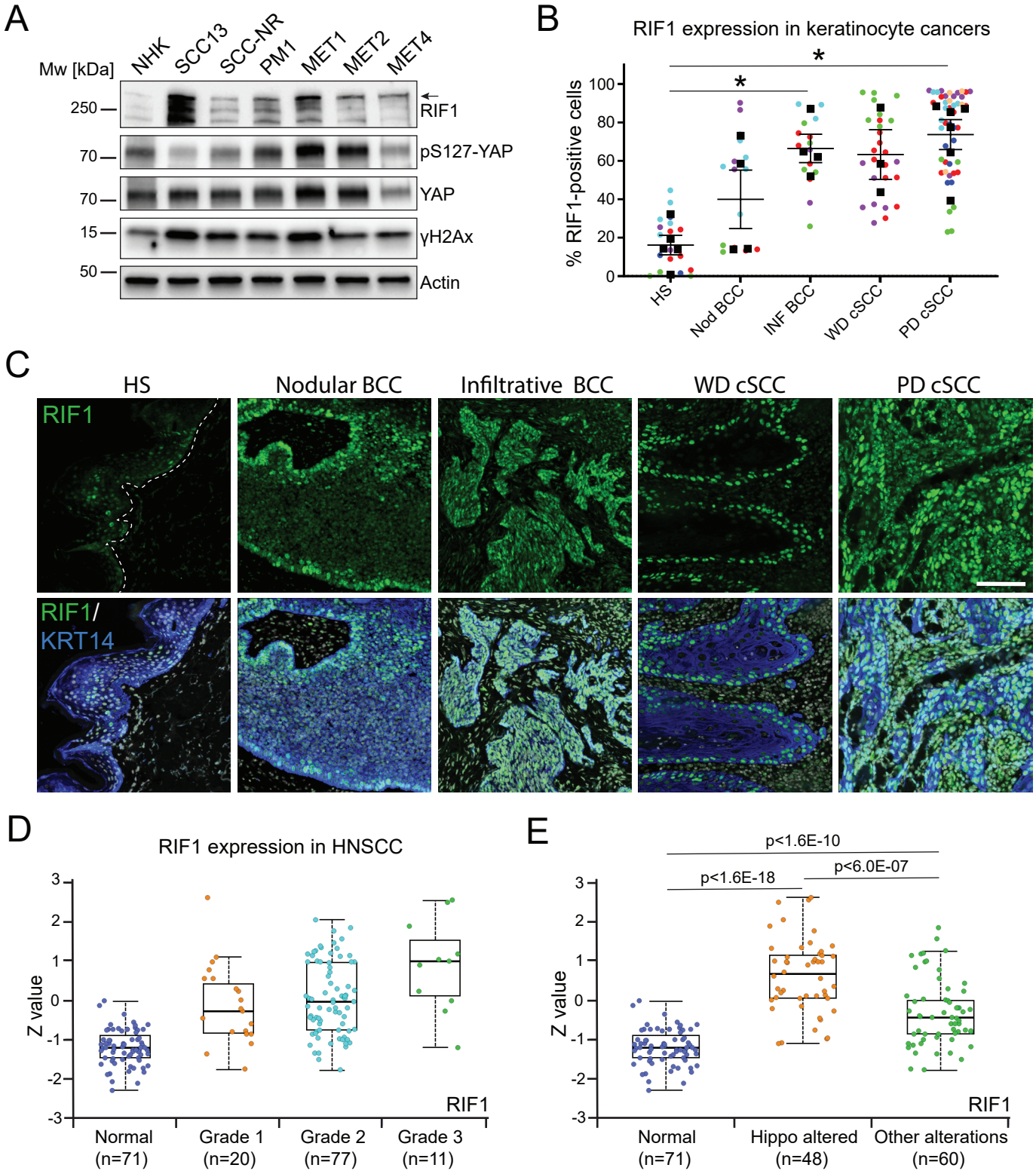

Figure 5_Bojko et al.

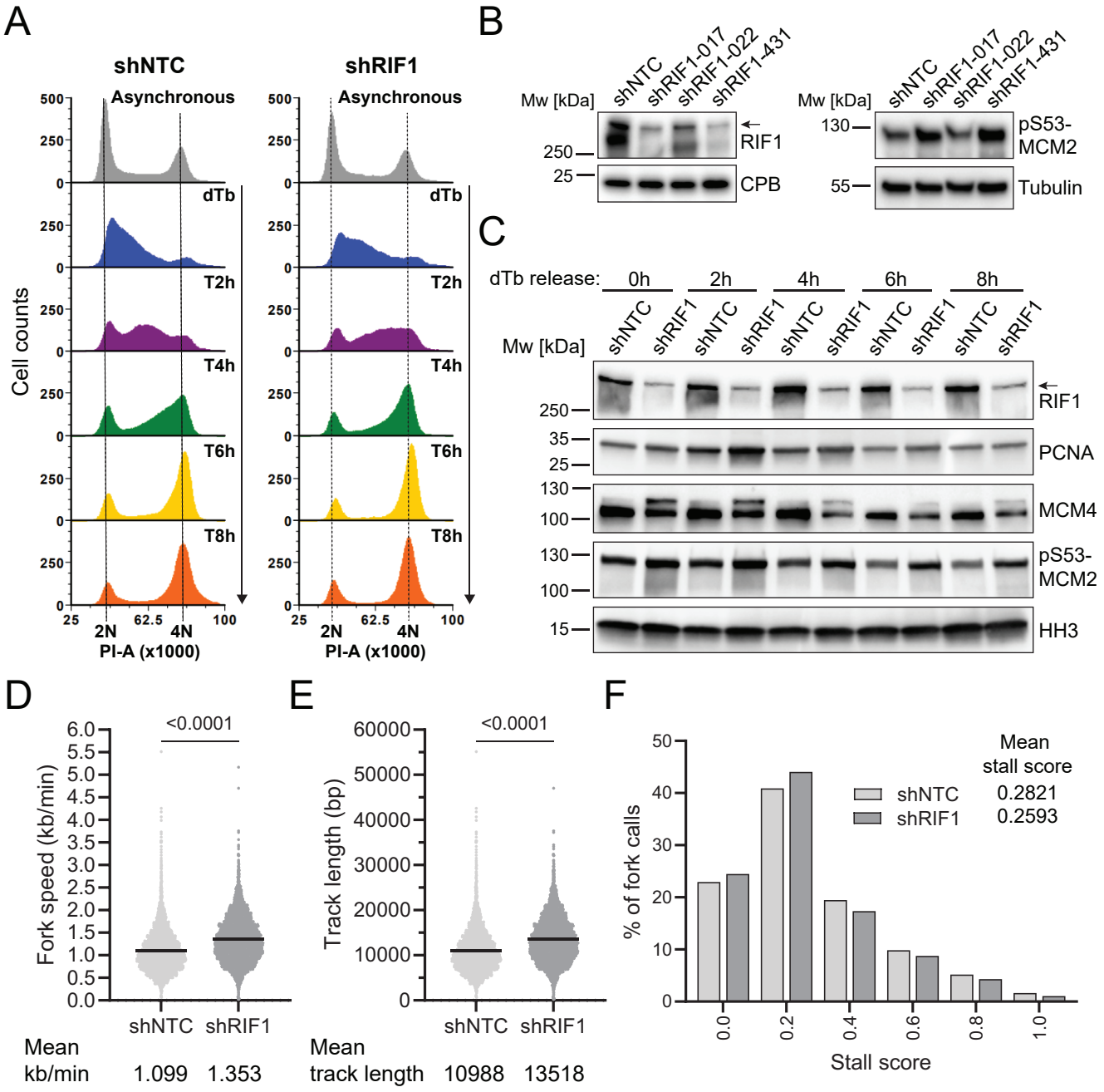

Figure 6_Bojko et al.

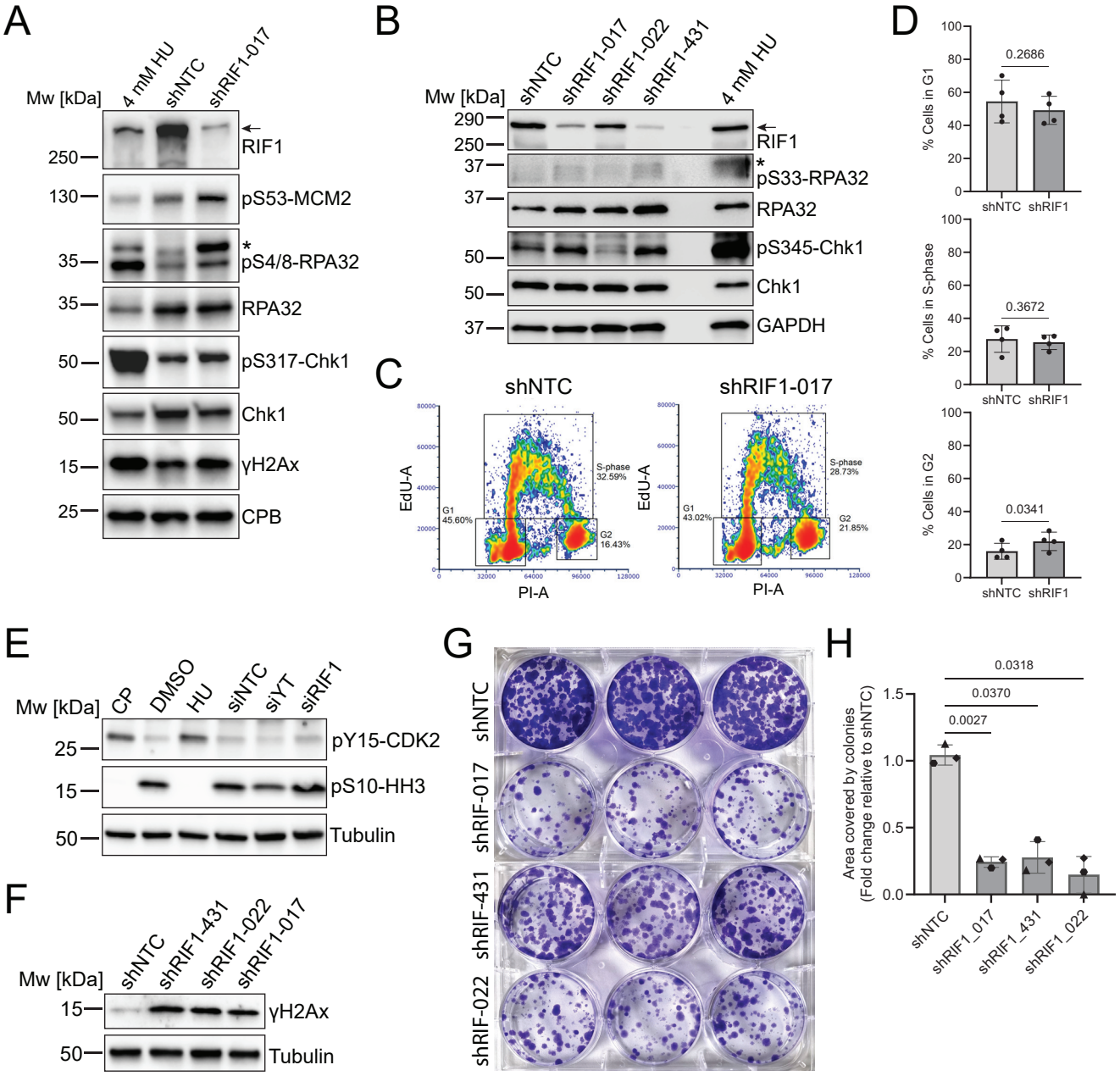

Figure 7_Bojko et al.

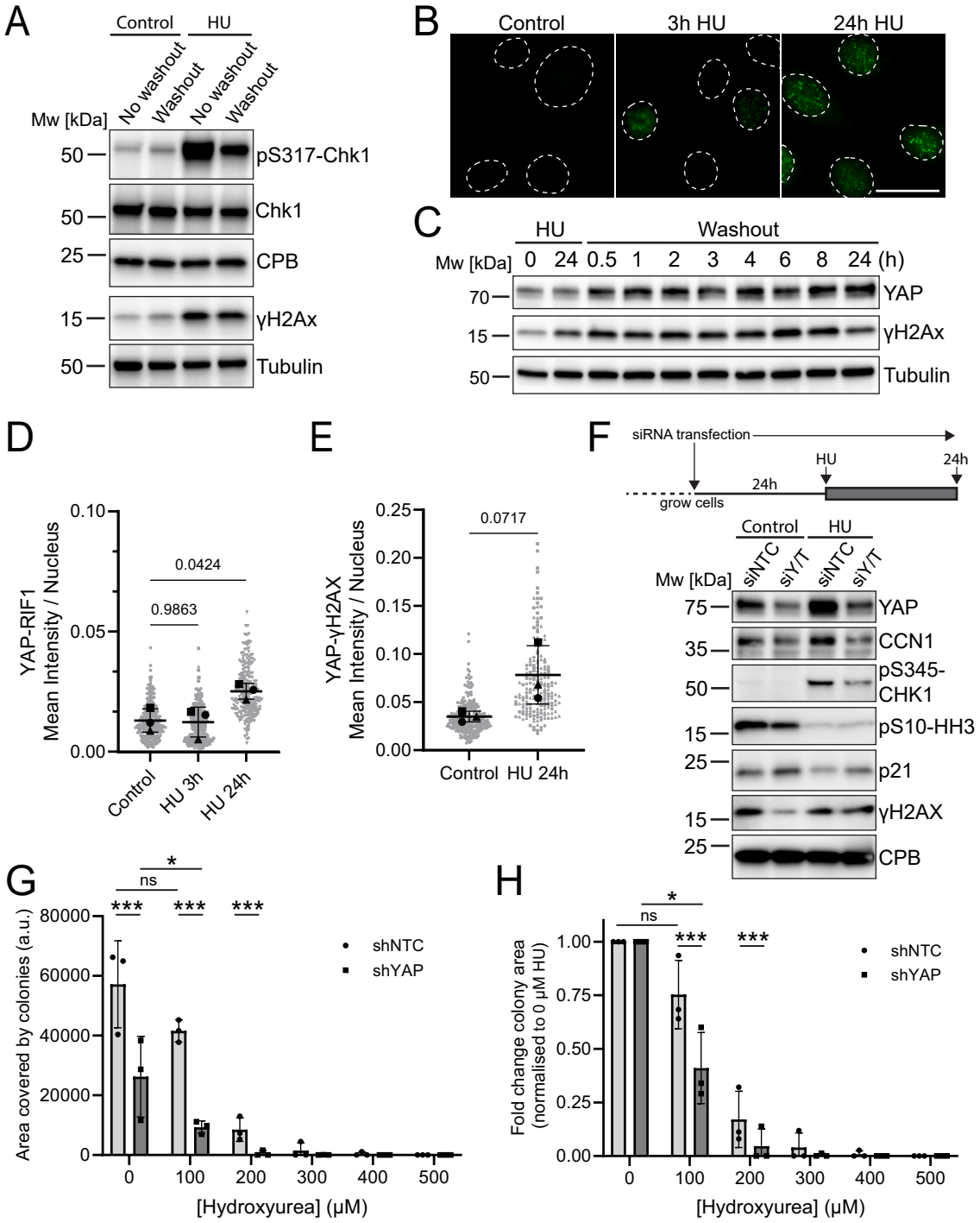

Figure 8_Bojko et al.